iScience

Article

Salivary gland cancer organoids are valid for preclinical genotype-oriented medical precision trials

Salivary Gland Cancer

Organoid Culture

Histopathology

Exome and Transcriptome
→Candidate Targetable Molecules

In vitro Testing for Genotype-oriented
Candidate Targeted Medicine
→**Precision Medicine**

Validation of Genotypes and Phenotypes

Tomohiko
Ishikawa, Takenori
Ogawa, Masahiro
Shiihara, ..., Kengo
Kinoshita, Yukio
Katori, Toru
Furukawa

toru.furukawa@med.tohoku.
ac.jp

Highlights
Organoids were
established from patient-
derived various salivary
gland cancers

Organoids retained most
histological and genetic
profiles of primary tumors

Organoids retained
heterogeneity and
experienced clonal
selection during culture

Organoids were a superior
in vitro model for testing
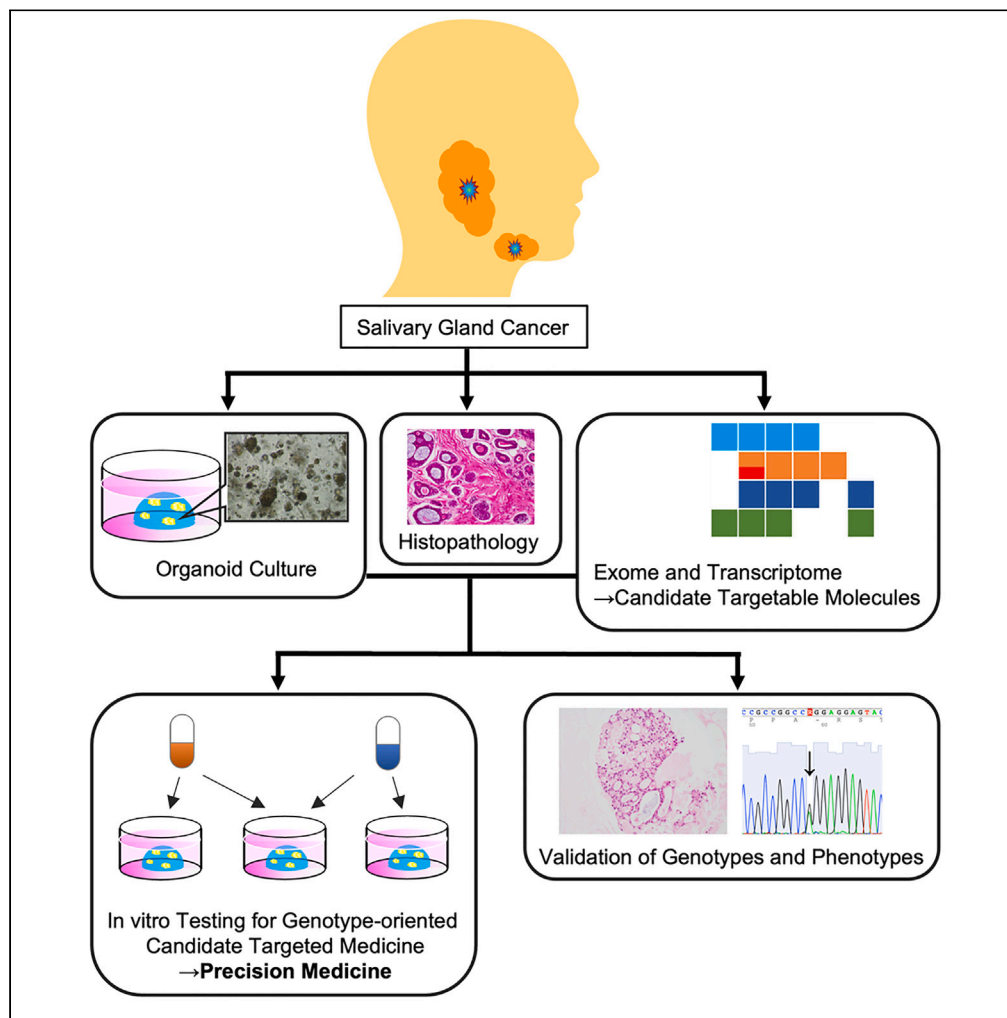genotype oriented
medicines

Article

Salivary gland cancer organoids are valid for preclinical genotype-oriented medical precision trials

Tomohiko Ishikawa,[1,2] Takenori Ogawa,[3] Masahiro Shiihara,[2] Hajime Usubuchi,[4] Yuko Omori,[2] Katsuya Hirose,[2] Taito Itoh,[2] Takuya Yoshida,[1,2] Ayako Nakanome,[1] Akira Okoshi,[1] Kenjiro Higashi,[1] Ryo Ishii,[1] Masahiro Rokugo,[1] Shun Wakamori,[1] Yasunobu Okamura,[5,6] Kengo Kinoshita,[5,6,7] Yukio Katori,[1] and Toru Furukawa[2,8,*]

SUMMARY

Salivary gland cancers (SGCs) are heterogeneous tumors, and precision oncology represents a promising therapeutic approach; however, its impact on SGCs remains obscure. This study aimed to establish a translational model for testing molecular-targeted therapies by combining patient-derived organoids and genomic analyses of SGCs. We enrolled 29 patients, including 24 with SGCs and 5 with benign tumors. Resected tumors were subjected to organoid and monolayer cultures, as well as whole-exome sequencing. Organoid and monolayer cultures of SGCs were successfully established in 70.8% and 62.5% of cases, respectively. Organoids retained most histopathological and genetic profiles of their original tumors. In contrast, 40% of the monolayer-cultured cells did not harbor somatic mutations of their original tumors. The efficacy of molecular-targeted drugs tested on organoids depended on their oncogenic features. Organoids recapitulated the primary tumors and were useful for testing genotype-oriented molecular targeted therapy, which is valuable for precision medicine in patients with SGCs.

INTRODUCTION

Salivary gland cancers (SGCs) are rare and heterogeneous tumors that account for less than 10% of all head and neck cancers.[1] SGCs consist of 20 pathological types according to the World Health Organization (WHO) Classification of Head and Neck Tumors,[2] and molecular profiles and clinical behaviors of SGCs vary depending on the type. High-grade malignancies such as salivary duct carcinoma (SDC) and adenoid cystic carcinoma (AdCC) are known to cause distant failure in 40%–50% of cases,[3,4] which demands effective systemic therapy. To this point, limited case numbers, limited access to patient samples, and scarce availability of authenticated cell lines and animal models have impeded our understanding of the pathobiology of SGCs and the development of effective targeted therapies.[5] Comprehensive genomic profiling, such as whole-exome sequencing (WES), has been used to identify effective therapeutic strategies for precision medicine.[6,7] Recent studies have uncovered the molecular profiles of SGCs, including aberrations in *TP53*, the cyclin pathway, the PI3K/AKT/mTOR pathway, *HRAS*, *BAP1*, and *ERBB2*.[8–10] In addition, many types of SGCs harbor fusion genes, some of which are considered targetable alterations; however, the impact of precision medicine on SGCs has not yet been proven. Organoid culture is an *in vitro* three-dimensional culture that can preserve the *in vivo* tissue-specific structures and functions.[11] Cancer organoids derived from patients' tumors are supposed to be superior to conventional monolayer cultures in terms of their homology to the tumor nature *in vivo*. Thus, cancer organoids may represent an ideal clinical model for tumors, such as a drug response-testing platform.[11,12] This study aimed to establish a translational model for testing molecular-targeted therapy by combining patient-derived organoids and genomic analyses for effective precision medicine in patients with SGCs.

RESULTS

Establishment of organoids from salivary gland tumor specimens

Twenty-nine patients, including 16 men and 13 women with an average age of 52.1 years, were enrolled in this study (Table S1). The primary sites were the parotid gland in 19 cases, the submandibular gland in five

[1]Department of Otolaryngology-Head and Neck Surgery, Tohoku University Graduate School of Medicine, Sendai 980-8574, Japan

[2]Department of Investigative Pathology, Tohoku University Graduate School of Medicine, Sendai 980-8575, Japan

[3]Department of Otolaryngology, Gifu University Graduate School of Medicine, Gifu 501-1194, Japan

[4]Department of Pathology, Sendai Kousei Hospital, Sendai 980-0873, Japan

[5]Tohoku University Advanced Research Center for Innovations in Next-Generation Medicine, Sendai 980-8573, Japan

[6]Tohoku University Tohoku Medical Megabank Organization, Sendai 980-8573, Japan

[7]Tohoku University Graduate School of Information Sciences, Sendai 980-8579, Japan

[8]Lead contact

*Correspondence: toru.furukawa@med.tohoku.ac.jp

https://doi.org/10.1016/j.isci.2023.106695

cases, the maxilla in three cases, the external ear in one case, and undetermined in one case. The pathological types included eight SDCs, six AdCCs, five mucoepidermoid carcinomas (MECs), four pleomorphic adenomas (PAs), and each one of acinic cell carcinoma (AciCC), basal cell adenocarcinoma (BCAC), carcinoma showing thymus-like differentiation (CASTLE), secretory carcinoma (SC), squamous cell carcinoma (SCC), and Warthin tumor (WT). The case of CASTLE was reported previously.[13] The average tumor size was 31.0 mm. Tumor samples were collected from primary tumors in 27 cases and neck lymph node metastases in two cases (cases 18 and 27). Biopsy specimens were also subjected to culture in MECs (cases 16 and 22), SDC (case 24), and PA (case 26).

We established organoids and monolayer cultured cells (two dimensional [2D] cells) from surgically resected primary tumors and biopsy specimens (Figure 1, Tables 1, S2, and S3). The success rates for obtaining passageable organoids and 2D cells were 72.4% (21/29) and 65.5% (19/29), respectively (Table 1). Among these tumors, the success rate for carcinoma tissues was 70.8% (17/24) for organoids and 62.5% (15/24) for 2D-cells. In some cases, most of spread cells in 2D culture did not grow as adherent cells to the dish and kept floating with forming spheroids in the culture medium. We collected such floating spheroids and submitted to organoid culture. Although most of such cells failed to grow in the matrix as well, one case showed successful establishment of organoids (Figure S1). The failure to obtain organoids was because of the contamination in three cases, absence of tumor cells in one case, handling errors in one case, and unknown without obvious technical errors in three cases. The failure to obtain 2D cells was because of contamination in four cases, absence of tumor cells in one case, handling errors in one case, and unknown without obvious technical errors in four cases.

The success rates for obtaining organoids and 2D cells from biopsy specimens were 25% (1/4) and 50% (2/4), respectively (Table S3, Figure S1). The failure to obtain organoids was because of contamination in two cases and unknown without obvious technical errors in one case. The failure to obtain 2D cells was because of contamination in one case and unknown without obvious technical errors in one case.

We optimized the culture conditions to be suitable for SGC organoids. We tested three types of culture media as follows: (1) full medium containing R-spondin, Wnt, and Noggin as described previously;[14] (2) full medium without R-spondin, Wnt, and Noggin; and (3) full medium without epidermal growth factor (EGF) (Figure S2). These modifications were made because the SGCs dependency on R-spondin, Wnt, Noggin, and EGF was unclear. We found that the medium without R-spondin, Wnt, and Noggin was superior to the full medium or the medium without EGF for the proliferation and sustainment of organoids in most cases. The medium without R-spondin, Wnt, and Noggin enabled organoids to grow continuously than other media in most of the cases although the full medium or the medium without EGF showed that a few organoids expanded in relatively bigger sizes initially; however, they failed to achieve more number of organoids (Figure S2).

In our series of organoids, most of organoids were cultured less than 10 passages and stocked in liquid nitrogen after being used in various assays. Although we did not test explicitly how long the organoids would continue to grow in serial passages, we confirmed that cases 9 (PA), 11 (SDC), and 29 (SDC) maintained expansion after 10 passages.

Tumor-derived organoids retained histopathology of their parental tumors

Organoids showed a spheroid formation with various appearances (Figure 1A). Tumor-derived organoids retained the histopathological features of their primary tumors (Figures 1B and S3). Organoids from AdCCs showed a cribriform structure with secretion of myxoid substances and expression of type IV collagen. The organoid from well-differentiated SCC (case 2) formed well-keratinized spheroids. The organoid from AciCC (case 3) consisted of acinic cells. Organoids from MECs (cases 8 and 18) showed variations as follows: The organoid from case 8 formed relatively large spheroids consisting of PAS-positive amorphous cells with few mucus droplets with weak CK7 and strong CK14 expression, suggesting that squamoid cells mainly grew.[15] In contrast, the organoids from case 18 were composed of diverse cells expressing CK7 and CK14, including those forming relatively small spheroids and those containing abundant mucus without forming clusters. The organoid from SC (case 10) formed small spheroids consisting of mucinous cells expressing S-100. The organoid from BCAC (case 13) consisted of palisading basal cells expressing p63. The organoid from PA (case 9) showed pleomorphism with occasional ductal formation and focal expression of p63. The primary tumor cells of case 8 revealed break-apart signals, indicating a translocation
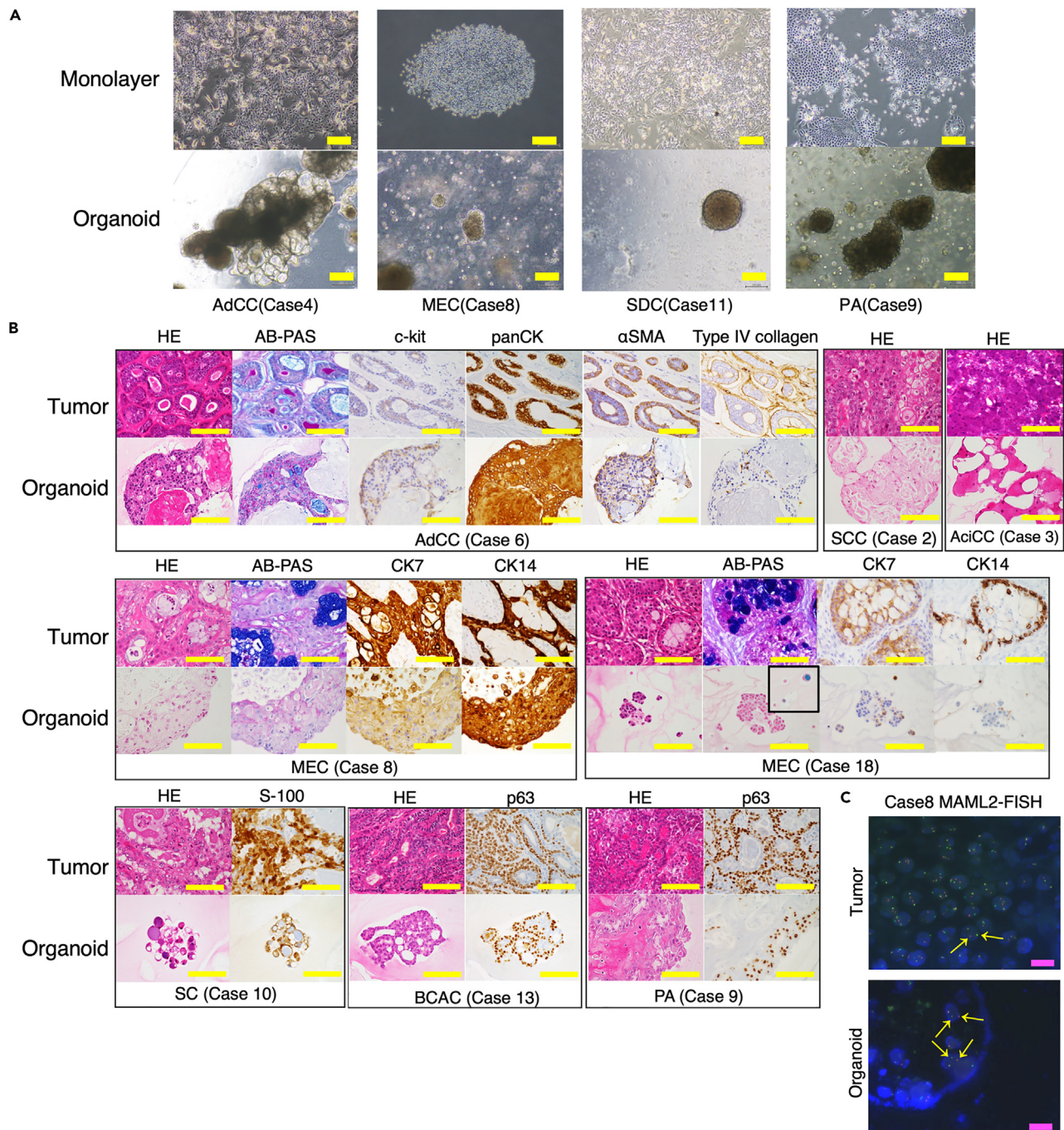
Figure 1. Tumor-derived organoids retained histopathology of the parental tumors

(A) Images of cultures. Upper and lower panel shows monolayer culture cells and organoids, respectively.

(B) Histopathological features of organoids derived from various salivary gland tumors. In each box of cases, upper panels and lower panels show features of original primary tumors and organoids, respectively.

(C) MAML2-FISH images of case 8 detected translocation of *MAML2* both in the primary tumor and organoids. Scale bars are 100 μm for culture and histological images, and 10 μm for FISH images. Abbreviations are AB-PAS, Alcian blue and periodic acid-Shiff double staining; FISH, Fluorescent *in situ* hybridization; and HE, hematoxylin and eosin staining. See also Figure S3.

of *MAML2* in fluorescent *in situ* hybridization (FISH) analysis, which was well retained in the derived organoid (Figure 1C). SGC organoids showed the strong expression of CD44, a marker of cancer stem cells[16] (Figure S3).

Table 1. Salivary gland tumors subjected for culture

Pathology	Number of samples	Number of passageable cultures obtained	
		Organoid	2D-cells
Salivary duct carcinoma	8	4	5
Adenoid cystic carcinoma	6	4	4
Mucoepidermoid carcinoma	5	4	3
Pleomorphic adenoma	4	3	3
Acinic cell carcinoma	1	1	0
Basal cell adenocarcinoma	1	1	1
Carcinoma showing thymus-like differentiation	1	1	1
Secretory carcinoma	1	1	0
Squamous cell carcinoma	1	1	1
Warthin tumor	1	1	1
Carcinoma total	24	17 (70.8%)	15 (62.5%)
Total	29	21 (72.4%)	19 (65.5%)

See also Tables S2 and S3.

WES and fusion gene analysis to identify targetable molecules

To identify potential targetable molecules, we conducted WES analysis on 19 SGCs and, for comparison, on three benign tumors (six SDCs, four AdCCs, four MECs, two PAs, and each one of AciCC, BCAC, CASTLE, SC, SCC, and WT; Table S4). These 19 SGCs harbored 54.9 (5–204, median 36) nonsynonymous somatic mutations on average (Table S4). Among various pathological types of SGC examined in this study, SDCs harbored significantly more nonsynonymous somatic mutations than AdCCs (p = 0.015), and MECs harbored those in between them, i.e., the average number of mutations was 110 (41–204) in SDC, 26 (6–49) in AdCC, and 49 (21–92) in MEC.

Mutational signature analysis[17] showed a mixture of various signatures in each case, comprising a clock-like signature (Signature 1) and other distinctive signatures, which suggested contributions of multiple carcinogenic pathways in SGCs, including the defective homologous recombination repair pathway (Signature 3), defective DNA mismatch repair pathway (Signatures 6 and 15), APOBEC pathway (Signatures 2 and 13), and tobacco chewing (Signature 29) (Figure 1). Compared with pathological tumor types, AdCC and MEC showed significant contributions from Signatures 3 and 29, respectively. SDC showed contributions of Signatures 2, 3, and 16, depending on the case. The APOBEC pathway (Signatures 2 and 13) contributed to MEC (case 8) and SDC (case 28) (Figure 2A).
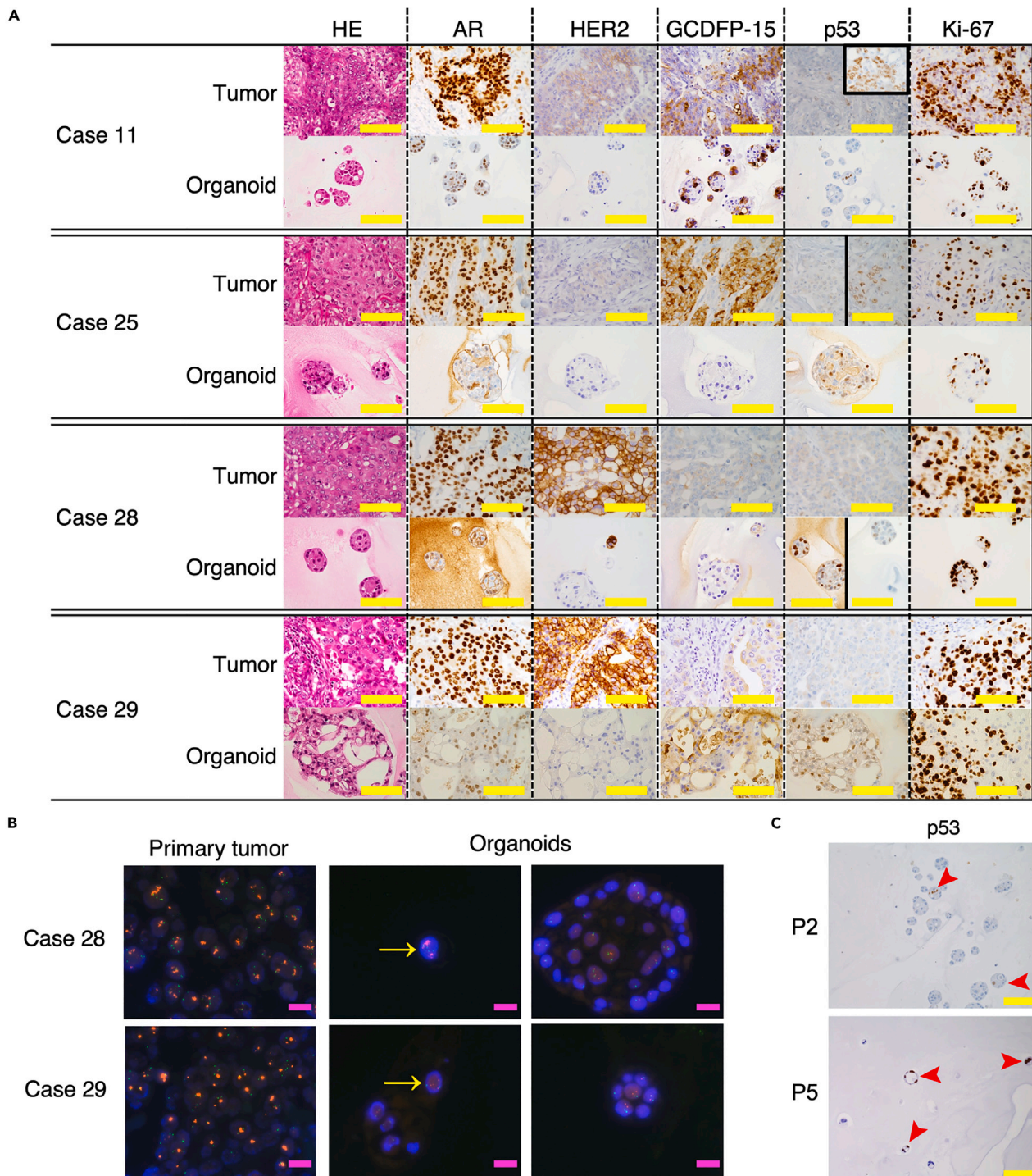
Somatic alterations, including copy number alterations (CNAs), were observed in multiple genes involved in canonical oncogenic signaling pathways, including the RAS, NRF2, PI3K, TGFβ, WNT, MYC, p53, cell cycle, Hippo, and Notch pathways (Figure 2B, Tables S5, S6, and S7). Candidate driver mutations were detected in 73% (14/19) of the cases (Table S5). Aberrations in the RAS signaling pathway were most frequently observed across various pathological types of SGCs, followed by those in the PI3K and Wnt pathways (Figure 2B).

SGCs are known to harbor various fusion genes, and indeed, we found *CRTC1* or *CRTC3* and *MAML2* fusions in all five cases of MEC, and *ETV6* and *NTRK3* fusion in a single case of SC (Figures 2B and 4A, Table S8).

Organoids retained case-dependent distinctive molecular features of salivary duct carcinoma

SDC organoids formed small solid spheroids with intracytoplasmic lumina in all cases, which preserved the histological characteristics of their original tumors (Figure 3A). Androgen receptor (AR) was expressed in all primary tumors and organoids; however, weaker expression was observed in organoids compared to that in primary tumors, especially in cases 25 and 28. HER2 expression in organoids showed variations compared to that in primary tumors. Organoids from primary tumors with weak (case 11, score 1+) or

Figure 2. WES and fusion gene analysis to identify targetable molecules in the primary tumor

(A) Proportions of mutation signatures detected by WES.

(B) Nonsynonymous mutations and copy number alterations classified into canonical oncogenic signaling pathways. See also Tables S4, S5, S6, S7, and S8.

null (case 25, score 0) HER2 expression, endorsed by no *HER2* amplification, consistently showed little HER2expression. In contrast, organoids from primary tumors showing strong HER2 expression (cases 28 and 29, score 3+) showed heterogeneity in HER2 expression; that is, some showed strong and others showed weak expression. HER2-FISH in these cases revealed that most primary tumor cells and a fraction of organoids harbored amplified *HER2* (Figure 3B). WES of the primary tumor in case 11 indicated wild-type *TP53*, which was consistent with the faint expression of p53 in most parts; however, focal overexpression of p53 was detected in this case. The organoid from this case showed an interesting phenotypic change in p53

Figure 3. Organoids retained the pathological difference between cases of salivary duct carcinoma

(A) Comparison of histopathological features of SDC cases. In each box of cases, upper panels and lower panels show features of original primary tumors and organoids, respectively.

(B) Fluorescent *in situ* hybridizations (FISH) to detect HER2 amplifications in primary tumors and organoids. Red and green signals indicate HER2 and 17-centromere, respectively. Note that most cells in primary tumors appeared to have amplification of HER2 whereas a few of cells in organoids showed HER2 amplification (arrows).

(C) p53 positive organoid cells in case 11were more frequent in the later passage (P5, lower panel) than in the early passage (P2, upper panel). Arrowheads indicate p53-positive clusters. Scale bars are 100 μm and 10 μm for histological images and for FISH images, respectively.

expression during the course of culture, that is, organoids with p53 overexpression were very few in an early passage (P2); however, these changes became apparent in a later passage (P5) (Figure 3C). WES of the primary tumor in case 25 showed a missense mutation of *TP53*, p.Arg181His, at a low frequency (variant allele frequency [VAF]: 0.08). Consistent with this finding, the tumor showed focal overexpression of p53, whereas the organoids showed no obvious overexpression. WES of primary tumors of cases 28 and 29 showed protein-truncated mutations of *TP53*, namely, p.Asn239fs (VAF: 0.54) in case 28 and p.Ser185fs (VAF: 0.38) in case 29. Immunohistochemistry showed that these tumors showed complete absence of p53 expression in most parts, whereas their organoids showed a mixture of clusters of cells with absent or faint expression of p53. These results indicate that organoids may retain the heterogeneity of their primary tumors and acquire phenotypic changes by spontaneous selection.

WES of culture cells uncovered unappreciated mutations in primary tumors

We examined whether cells in organoids and 2D cultures retained, gained, or lost somatic alterations compared to primary tumors. First, we examined whether mutations, including fusion genes, found in primary tumors were retained in organoids and 2D cells. We found that organoids significantly retained somatic mutations more often than 2D cells (Organoids versus 2D cells: 87.2% [50%–100%] versus 47.7% [0%–100%], p = 0.005). A total of 40% (6/15) cases of the 2D cells did not harbor any somatic mutations detected in their original tumors. Fusion genes were well retained in both organoids and 2D cells (Figure 4A, Table S8). Next, to obtain more comprehensive molecular profiles, we performed WES analyses for organoids and 2D cells of case 8 (MEC), case 11 (SDC), and case 18 (MEC). We compared highly confident somatic nonsynonymous variant calls by filtering out those of less than 0.1 in VAF or 10 in read counts in this analysis. WES revealed that both the organoid and 2D cells of case 11 retained all (55/55) of the mutations found in the primary tumor. In contrast, the organoid and 2D cells of case 8 retained only 10% (7/69) of the mutations found in the primary tumor. In case 18, the organoid retained all (29/29) of the mutations found in the primary tumor; however, 2D cells retained only 17% (5/29) of the mutations (Figure 4B). VAFs of these mutations commonly shared among primary tumors, organoids, and 2D cells generally showed higher frequencies in primary tumors than those not commonly shared, which indicated that major mutations in primary tumors were well preserved in organoids and 2D cells, even in case 8 (Figure 4C and Video S1). However, among the major mutations in primary tumors, some were lost in organoids and/or 2D cells in a chromosome-specific manner, in which variants on the chromosome X in primary tumors were lost in 2D cells in two cases (cases 8 and 18) and in the organoid in one case (case 8). Strikingly, WES of organoids and 2D cells uncovered mutations that were undetected in the corresponding primary tumors. Moreover, these "gained" mutations were observed in organoids more often than in 2D cells (Figure 4B, Tables S9, S10, and S11). The most remarkable example of this phenomenon was a missense mutation in *TP53* (p.Cys176Phe; VAF: 0.98) detected only in the organoid, but not in the primary tumor nor 2D cells in case 11 (Figure 4B, Table S10). As we showed in the histological analysis, the primary tumor in this case focally showed overexpression of p53, and the organoid showed an increase in cells with p53 overexpression in later passages in comparison with early passages of cell culture (Figure 3C). This suggests that tumor cells harboring *TP53* mutations existing as a minor population in the primary tumor may be selected to grow during the course of the organoid culture, but not in the 2D culture. The copy number variation profiles of primary tumors resembled those of organoids more than 2D cells except for case 8 (Figure 4D). The mutational signatures of primary tumors seemed to be well preserved in organoids and 2D cells (Figure S4). Comparison of molecular profiles between early- and later-passaged organoids in case 11 showed almost identical profiles (Figure S4). These results indicate that major mutations in primary tumors are likely to be retained in both organoids and 2D cells; however, organoids can harbor more diverse tumor cells with distinct mutations than 2D cells, which may signify the superiority of organoids compared to 2D cells in addressing the diverse nature of primary tumors.

Organoids retained transcriptome profiles compared with primary tumors with characteristic modifications

We performed a transcriptome sequencing analysis to know gene expression profiles among primary tumors, organoids, and 2D cells of cases 6 and 11. The transcriptome revealed that organoids and 2D cells retained the expression profile of their primary tumors (Rho values of organoid versus tumor, 2D cells versus tumor, and organoid versus 2D cells were 0.86, 0.88, and 0.93 in case 6; and 0.84, 0.85, and 0.93, respectively, in case 11) (Figures 4E and 4F, Table S12). The *MYB-NF1B* fusion gene detected in the primary tumor of case 6 as a characteristic phenotype of AdCC was confirmed to be retained and expressed in its organoid and 2D cells. In addition, there are some significant differences between primary tumors and organoids/2D
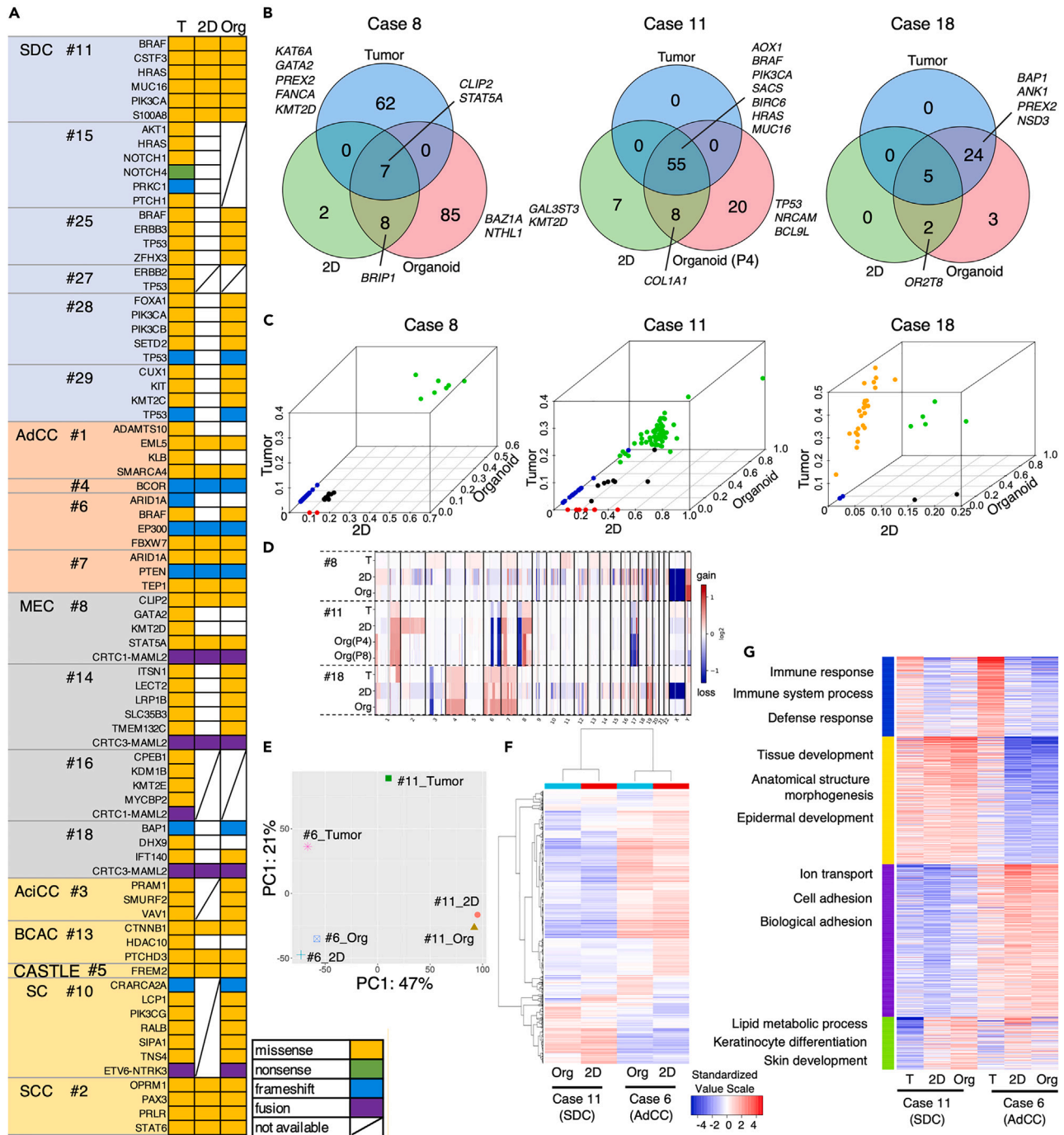
Figure 4. Comparison of genetic profiles of organoids, 2D cells, and parental tumors

(A) Comparison of validated mutations through Sanger sequencing in primary tumors, 2D cells, and organoids. Blank boxes indicate that mutations were not detected upon validation. Strikethrough marks mean that data was not available because of unavailability of cultured cells for validation.

(B–D) WES analysis of cultured cells from cases 8, 11, and 19. (B) Venn diagrams showing somatic mutations in the primary tumor, 2D cells, and organoids in each case. Genes indicated are possible cancer driver genes. (C) Three-dimensional scatterplots of somatic mutations according to variant allele frequency. (D) A heatmap of copy number alterations on global chromosome in the primary tumor, 2D cells, and organoids.

(E–G) Data analyses of transcriptome sequencing of organoids, 2D cells and primary tumors of cases 6 and 11. (E) Principal component analysis indicating closely related data points. (F) A heatmap indicating hierarchical clustering of expression levels. (G) A heatmap by K-means clustering according to ontologies. The top representative three ontologies are indicated in each cluster. Abbreviations are 2D, 2D cells; Org, organoids; and T, primary tumor. See also Figure S4 and Tables S8, S9, S10, S11, S12, and S13.
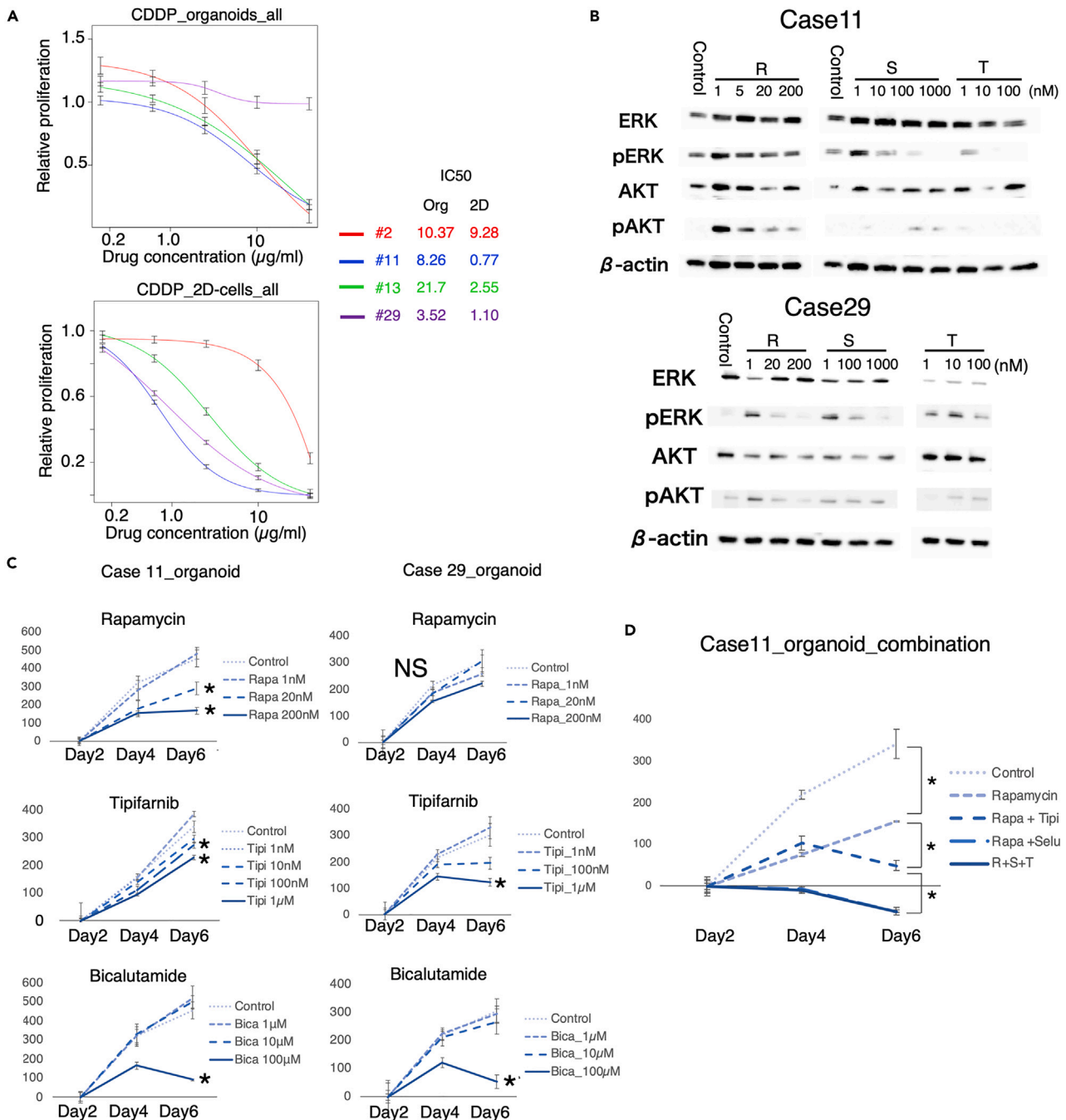
cells. Enrichment analysis revealed that primary tumors showed significantly higher expression of genes related to immunity and responses to stimuli. In contrast, organoids/2D cells showed significantly higher expression of genes related to metabolic processes, and keratinocyte/epidermal/epithelial differentiation (Figure 4G, Table S13). These results suggest that tumor cells of epithelial lineage selectively proliferate in cultures without immune cells. Comparison of the expression between organoids and 2D cells revealed that five genes were significantly differentially expressed, *GDF15* and *AKR1C2* were downregulated and *RAB3B*, *PPFIA4*, and *IGFBP5* were upregulated in organoids (Figure S4). The organoids showed significantly higher expression of genes in pathways associated with cell division, mitotic spindle organization, chromosome segregation, nucleosome assembly and organization, and DNA conformational change, and lower expression of genes in pathways associated with ribosome biogenesis, non-coding RNA processing, mitochondrial translation/gene expression, catabolic processes of organic acids and carboxylic acids, and the signal-recognition particle-dependent proteins targeting the membrane (Table S14). These results suggest that organoids may have higher activity in cell division and are less active in protein synthesis and catabolic processes.

Established monolayer and organoid cells are applicable for drug sensitivity test

SGC organoids established from primary tumors are likely to be an ideal *in vitro* model for testing drugs, including drugs for molecular targets identified by WES. First, we examined the sensitivity of organoids from various types of SGC, namely, AdCC (cases 1 and 6), SCC (case 2), SDC (cases 11 and 29), and BCAC (case 13), to the conventional chemotherapeutic drug cisplatin. According to clinical aggressiveness, SDCs (cases 11 and 29) proliferated more rapidly than those of other tumor types (Figure S4). Cisplatin inhibited organoid proliferation in a dose-dependent manner in all cases, whereas the organoid in case 29 was resistant to cisplatin. We compared responses to cisplatin between organoids and 2D cells from the same parental tumor, which revealed that 2D cells were more sensitive to cisplatin than organoids, that is, IC50 (μg/mL) in organoids and 2D cells were 10.37 and 9.28 in case 2, 8.26 and 0.77 in case 11, 21.79 and 2.55 in case 13, and 3.52 and 1.10 in case 29, respectively (Figures 5A and S5).

Molecular targeted therapy based on WES efficiently inhibited the growth of organoids from SDC

Next, we tested genotype-oriented molecular-targeted drug candidates in SDC cases. In the primary tumor of case 11, oncogenic mutations of *PIK3CA* p.H1047R, *HRAS* p.Q61R, and *BRAF* p.N581I were identified by WES, indicating that activation of the PI3K/AKT/mTOR and MAPK pathways played a driver's role in this case. Therefore, we tested targeted therapeutics including rapamycin, an mTOR inhibitor; tipifarnib, a farnesyltransferase inhibitor that prevents HRAS activation; and selumetinib, an MEK inhibitor that blocks the MAPK pathway. We also tested AR inhibitor bicalutamide and the humanized anti-HER2 antibody trastuzumab because the tumor expressed AR strongly and HER2 weakly (Figure 3A), which suggested that bicalutamide would have a superior effect than trastuzumab in this case. We also tested these drugs in the organoid of case 29, whose primary tumor did not harbor any remarkable mutations in the PI3K or RAS/MAPK pathways, but showed strong expression of both AR and HER2 with gene amplification of *HER2*. However, the organoids barely showed HER2 expression or *HER2* amplification (Figures 3A and 3B). In the organoids of case 11, immunoblotting demonstrated that rapamycin downregulated phosphorylated AKT (pAKT) in a dose-dependent manner without affecting ERK activity. In this case, selumetinib downregulated phosphorylated ERK (pERK) and upregulated pAKT in a dose-dependent manner. Tipifarnib also downregulated pERK in a dose-dependent manner, without affecting AKT activity. In the organoids of case 29, rapamycin downregulated both pAKT and pERK, selumetinib downregulated pERK without affecting AKT activity, and tipifarnib downregulated pERK and upregulated pAKT in a dose-dependent manner (Figure 5B). In the proliferation assay of the organoids in case 11, these targeted drugs inhibited organoid growth in a dose-dependent manner, that is, rapamycin (20 nM or above), tipifarnib (100 nM or above), and bicalutamide (100 μM) significantly inhibited organoid growth (Figures 5C and S5–S7). These responses to the drugs were different from those in case 29 in some respects. Although tipifarnib (1 μM) and bicalutamide (100 μM) significantly inhibited organoid growth, rapamycin did not significantly inhibit growth (Figures 5C, S6, and S7). Selumetinib and trastuzumab did not inhibit organoid growth significantly in either case. 2D cells from case 11 and organoids from PA (case 9) were also examined, 2D cells from case 11 showed similar responses to their organoids, whereas drugs did not significantly inhibit the growth of organoids in case 9 (Figures S6 and S7).

A

CDDP_organoids_all

CDDP_2D-cells_all

	IC50	
	Org	2D
#2	10.37	9.28
#11	8.26	0.77
#13	21.7	2.55
#29	3.52	1.10

B

Case11

Case29

C

Case 11_organoid   Case 29_organoid

D

Case11_organoid_combination

Figure 5. Drug sensitivity test using organoids

(A) Dose-response curves of organoids (upper panel) and monolayer culture cells (lower panel) of cisplatin treatment in cases 2, 11, 13 and 29.

(B) Immunoblots after treatment with molecular targeted drugs.

(C) Proliferation assays of organoids treated with molecular targeted drugs in cases 11 and 29.

(D) Relative proliferation of case 11 after the combination therapy. *p < 0.05 in Student's *t* test. Abbreviations are NS, no significance; R, rapamycin; S, selumetinib; T, tipifarnib. Data are represented as mean ± SEM. See also Figures S5–S8.

Synergistic effects of the combination of PI3K pathway and MAPK pathway inhibition

We investigated the efficacy of combined therapy targeting both PI3K/AKT/mTOR and MAPK pathways using 20 nM rapamycin with 1 μM selumetinib and 100 nM tipifarnib. In case 11, this combination synergistically inhibited organoid growth (control versus rapamycin, p = 0.0012; rapamycin versus rapamycin +

tipifarnib, p = 0.0028; rapamycin versus rapamycin + selumetinib, p = 0.010; Figure 5D). In addition, selumetinib showed a stronger inhibitory effect than tipifarnib, and the addition of tipifarnib to rapamycin + selumetinib did not affect organoid growth (rapamycin + tipifarnib versus rapamycin + selumetinib: p = 0.023; rapamycin + selumetinib versus rapamycin + selumetinib + tipifarnib: p = 0.98). In case 29, the addition of rapamycin or selumetinib to tipifarnib did not show a synergistic inhibitory effect compared to tipifarnib monotherapy (Figure S7).

DISCUSSION

Tumor-derived organoids have been established for many cancers; however, limited studies have been reported regarding SGC organoids. Keysar et al. demonstrated that they could culture cells forming spheroids *in vitro* from xenografts of patient-derived MEC, AdCC, and AciCC cases.[16] Similarly, Takada et al. reported that they established organoids from patient-derived xenografts of AdCCs, although they experienced difficulties in expanding organoids because of their slow growth.[18] Alamri et al. demonstrated successful organoid and 2D cultures of MEC and PA, in which the MEC organoid was used in a drug sensitivity test, although the MEC they used did not harbor the *CRTC1/3-MAML2* fusion gene, which is common for most MECs.[19] In our study, we succeeded in establishing and expanding organoids directly from patients' tumor tissues in a variety of histological types, and demonstrated that these organoids were useful for drug sensitivity tests based on genomic information examined by WES. We performed detailed comparative analyses of histological and molecular features among primary tumors, organoids, and 2D cells, which revealed that organoids retained the major mutations, including fusion genes, as well as miscellaneous heterogeneous mutations of primary tumors. In addition, we demonstrated that organoids have an advantage in retaining heterogeneity comparted to 2D cells. Moreover, organoids were uncovered to undergo selective/evolutional changes during culture. This information may add significant knowledge regarding the characteristics of SGCs-derived organoids and their usefulness as an *in vitro* model for precision medicine.

We tested several conditions for organoid cultures, and achieved sufficient modifications to establish passageable organoids from SGCs. It has been suggested that essential growth factors for obtaining organoids may depend on the organs of their origins.[11,20,21] We found that the medium without Wnt3a, Rspo1, and Noggin was most suitable for establishing organoids from SGCs. We initially hypothesized that the full medium containing Wnt3a, Rspo1, and Noggin would be the most appropriate medium for culturing organoids, as proved in several cancer organoids including pancreatobiliary cancers in our previous study.[14] The medium without Wnt3a, Rspo1, and Noggin is supposed to be suitable for tumors independent of exogenous Wnt pathway stimulation and bone morphogenic protein inhibition. In particular, Wnt pathway stimulation seems to be required for most of epithelial-lineage organoids, while some tumor organoids can grow in Wnt autonomy.[22] Surprisingly, unlike other cancers, most of organoids from SGCs grew best in the medium without Wnt, R-spondin, or Noggin. It is indicated that Wnt pathway activity is associated with the proliferation of AdCC cell line,[23] and the long-term expansion of salivary gland organoid.[24] Also, AdCC and MEC are demonstrated to express cyclin D-1 constantly,[25] a downstream molecule of Wnt pathway. These lines of evidence suggest that Wnt signaling activity is necessary for SGCs, either by exogenously or autogenously; however, our results indicated that most of SGCs are independent of exogeneous Wnt pathway stimulation. This autonomy could be because of self-activation of the Wnt pathway, most likely by mutations in Wnt pathway-associated genes. In our studied cases, mutations in Wnt pathway genes were frequent. Moreover, our results may also indicate that exogenous supplementation with Wnt3a, Rspo1, and Noggin inhibits the proliferation and survival of SGC organoids. Exogenous Wnt or R-spondin supplementation to cancer organoids with activating mutations of genes in the Wnt pathway typically does not result in poor organoid outgrowth[22,26]; therefore, the exact cause of this inhibition remains elusive. Nevertheless, our finding of a suitable medium may facilitate further research on SGC organoids. Our culture system seems particularly suitable for organoids of SDC because they grow faster than organoids of any other histological types, besides SDC is a very aggressive tumor, therefore, it might reflect its aggressiveness.

We also succeeded in obtaining organoids from the biopsy specimens. The establishment of organoids from needle biopsy specimens has been reported for various tumors. Considering their clinical use, establishing organoids from a biopsy is ideal because organoids can be obtained even from unresectable or metastatic lesions in situations that require systemic therapy. As head and neck cancers often arise in easy-to-access locations for biopsy, they are likely to be good candidates for designing precision medicine

utilizing organoids. However, the success rate of culture was low in this study mainly because of contamination, so we should apply more stringent sterile procedures such as extensive washing with anti-microbes of biopsy specimens.

We established 2D cells from six histological types of SGCs. The success rate of 2D cells was lower than that of organoids; this might be because of the culture conditions because we used the same medium used for organoid culture for 2D cell culture. Although rarely, we found that some floating cells that are usually assumed to be inappropriate for monolayer culture could form organoids, which may indicate that cells not adapting to 2D culture can grow as organoids. We checked the molecular features of 2D cells and found that some 2D cells did not harbor somatic mutations detected in their original tumors, which can be a pitfall for the preclinical testing. In particular, four SDCs and three MECs grew well in monolayer culture, but three of the four SDCs and two of the three MECs did not harbor somatic mutations found in their primary tumors. Our results may emphasize the importance of validating genetic alterations observed in primary tumors when testing drug sensitivity by applying primary cultured cells, especially in testing molecular-targeted therapy.

Although organoids retained most of the histopathological characteristics of their primary tumors, there were discrepancies in expression of HER2 and p53 in SDC cases. A previous study reported a similar discrepancy in HER2 expression between organoids and their primary tumors in breast cancer cases, and it was assumed that selected growth and genomic instability could have caused such discrepancy.[27] Another study of colorectal cancer organoids showed that organoids with chromosomal instability frequently had mitotic errors, followed by cell death.[28] These studies suggest that cells with chromosomal instability and amplified-*HER2* tend to fail to thrive because of mitotic errors in organoid cultures. Regarding p53, we observed a dynamic change in p53 expression in case 11, and WES analysis revealed that organoids harbored a *TP53* mutation with high VAF that was not detected in the primary tumor. Although we could not exclude the possibility that organoids acquired a novel mutation during culture, it is reasonable to consider that a small part of the primary tumor cells with *TP53* mutations selectively grew because a small part of the primary tumor showed overexpression of p53, as shown in Figure 3A. Comparison of WES analysis between early passaged (P4) and later passaged (P8) organoids demonstrated no significant difference, suggesting that the major difference between the primary tumor and the organoid occurred at an earlier time before P4. Pathological findings revealed that p53-positive cells increased from P2 to P5, suggesting that selection mainly occurred from P2 to P5. Although we could not perform this because tissues and nucleic acids were not always collected at each point, sequential genetic and histopathological analyses from the start point of culture may be required to investigate the dynamic changes in detail. These results also suggest that heterogeneity or clonal evolution in primary tumors can be reproduced in organoids. This may be particularly important when using organoids for drug testing because clonal selection by drugs frequently occurs in clinical settings and organoids may recapitulate this phenomenon. However, discrepancies in phenotypes between organoids and primary tumors are supposed to greatly influence the responses to drugs; therefore, checking molecular features may be necessary to evaluate and predict clinical outcomes.

We demonstrated the efficacy of candidate-targeted drugs selected based on oncogenic mutations detected by WES in patient-derived organoids. Pathway-specific inhibitors, namely, mTOR and RAS-MAPK inhibitors, proved to be effective for tumors with PI3K pathway mutations and RAS-MAPK pathway mutations. Moreover, the combined drugs showed synergistic effects, which may have increased the efficacy of the targeted drugs. The study of combined therapy is one of the great advantages of preclinical tests using organoids because such combinations occasionally result in unexpected effects. Previous studies have shown that simultaneous alterations in the RAS and PI3K pathways are commonly observed in SGCs,[8] and the independent use of PI3K pathway and RAS inhibitors for SGCs showed a limited effect.[29,30] In addition, MEK inhibitors are known to show off-target effects, activating the PI3K/AKT pathway, which may result in drug resistance.[31] Instead, because the synergistic effect of tipifarnib and AKT inhibitors combination for breast cancer has been reported,[32] our study also demonstrated the synergistic effect of this combination therapy.

Organoids from SDCs with strong expression of AR and weak HER2 expression responded to bicalutamide but not to trastuzumab, which was consistent with previous clinical studies, showing that androgen deprivation therapy and anti-HER2 therapy were particularly effective for AR-positive tumors and HER2-overexpressing tumors in SGCs, respectively.[33,34] Notably, 11.1% (4/36) and 14.0% (8/57) of cases showed complete response in AR deprivation therapy and anti-HER2 therapy, respectively, in previously published
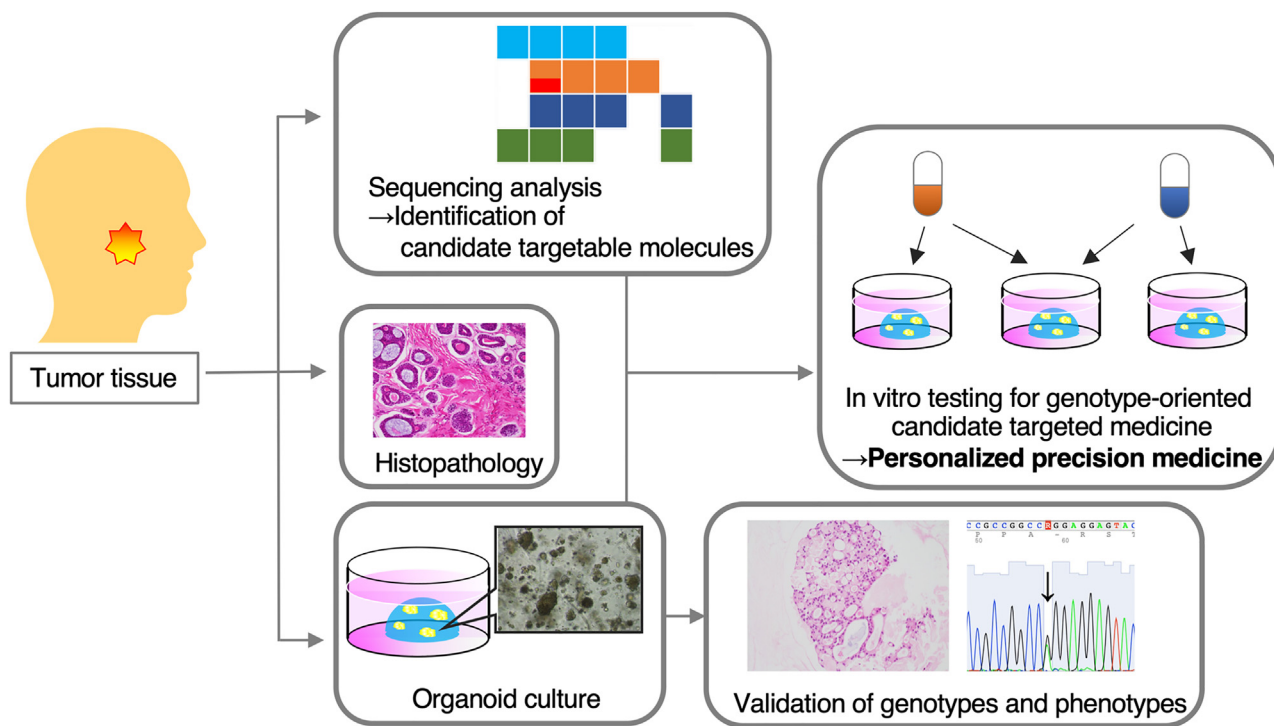
Figure 6. Schematic of precision medicine for SGCs based on organoids and comprehensive genetic analysis

studies,[33,34] suggesting that these therapies can be very effective in some patients. As biomarkers are needed to determine which patients are likely to benefit from other therapies, organoids can provide great help in the investigation of such biomarkers.

Although we were able to identify driver genetic alterations in 73% of SGCs using WES, some cases did not harbor any actionable mutations reported as drug targets. A previous study using panel sequencing reported that 40.6% (76/187) of the cases did not harbor actionable gene aberrations.[35] For cases without such actionable gene alterations, high-throughput drug screening in an *in vitro* model may indicate appropriate treatment strategies,[12] and organoids may be applied for such screening and expand the opportunity of precision medicine in SGCs. Organoids have also been reported to be useful in predicting radiation response;[36] screening for radiation response for our established organoids may provide useful information for the treatment of SGCs, which was not included in this study.

In conclusion, we have established organoids from various types of salivary gland tumors. Organoids of SGCs were superior to monolayer cultures in preserving the characteristics of patients' primary tumors, including their heterogeneity. Organoids are useful for validating activating oncogenic pathways and testing genotype-oriented molecular targeted therapies, which can serve to improve the efficacy of precision medicine for patients with SGCs (Figure 6).

Limitations of the study

First, it is difficult to determine whether our method for culturing organoids from SGC tissues is optimal or not because we did not examine the effect of each supplement in the culture medium on the growth of organoids. Second, because we performed experiments using early passaged cultures because turn-around time for giving clinically useful information should be very critical in presumed clinical situation, we did not investigate explicitly how long the cultured cells would continue to grow. Third, WES analysis of organoids and 2D cells was restricted to a few cases; therefore, the diversity of molecular phenotypes observed in this study may not be a general phenomenon. Fourth, we did not establish non-tumoral salivary gland organoids, which prevented us from determining whether the drugs were tumor-specific. Fifth, we did not obtain data on the clinical responses of the patients to the drugs evaluated in this study, which is an important theme to be clarified in the future.

STAR★METHODS

Detailed methods are provided in the online version of this paper and include the following:

- KEY RESOURCES TABLE
- RESOURCE AVAILABILITY
  - Lead contact
  - Materials availability
  - Data and code availability
- EXPERIMENTAL MODEL AND SUBJECT DETAILS
- METHOD DETAILS
  - Processing patients' materials
  - Organoid and monolayer cultures
  - WES and sanger sequencing
  - Whole transcriptome sequencing analysis
  - RT-PCR to detect fusion genes
  - Histopathology, immunohistochemistry, and fluorescent *in situ* hybridization (FISH)
  - Immunoblotting
  - Cell viability assay with patient-derived cancer organoids and monolayer culture cells
  - Imaging analysis
- QUANTIFICATION AND STATISTICAL ANALYSIS

SUPPLEMENTAL INFORMATION

Supplemental information can be found online at https://doi.org/10.1016/j.isci.2023.106695.

AUTHOR CONTRIBUTIONS

T. Ishikawa: Conceptualization, data curation, formal analysis, investigation, visualization, writing – original draft, **T.O.:** Conceptualization, funding acquisition, project administration, resources, supervision, **M.S.:** Investigation, methodology, **H.U.:** Investigation, **Y. Omori:** Investigation, writing – review and editing, **K.H.:** Investigation, **T. Ito**: Investigation, **T.Y.:** Investigation, resources, **A.N.:**Funding acquisition, resources, writing – review and editing, **A.O.:** Resources, writing – review and editing, **K.H.:** Resources, writing – review and editing, **R.I.:** Resources, writing – review and editing, **M.R.:** Resources, **S.W.:** Resources, **Y. Okamura:** Data curation, formal analysis, investigation, **K.K.:** Data curation, formal analysis, investigation, **Y.K.:** Project administration, supervision, **T.F.:** Conceptualization, data curation, funding acquisition, methodology, project administration, supervision, visualization, writing – review & editing.

DECLARATION OF INTERESTS

The authors declare no competing interests.

REFERENCES

1. Sung, H., Ferlay, J., Siegel, R.L., Laversanne, M., Soerjomataram, I., Jemal, A., and Bray, F. (2021). Global cancer statistics 2020: GLOBOCAN estimates of incidence and mortality worldwide for 36 cancers in 185 countries. CA Cancer J. Clin. 71, 209–249. https://doi.org/10.3322/caac.21660.

2. El-Naggar, A.K., Chan, J.K.C., Grandis, J.R., Takata, T., and Slootweg, P.J. (2017). WHO Classification of Head and Neck Tumours, 4th edition (IARC Press).

3. Mifsud, M., Sharma, S., Leon, M., Padhya, T., Otto, K., and Caudell, J. (2016). Salivary duct

carcinoma of the parotid: outcomes with a contemporary multidisciplinary treatment approach. Otolaryngol. Head Neck Surg. *154*, 1041–1046. https://doi.org/10.1177/0194599816636812.

4. Dodd, R.L., and Slevin, N.J. (2006). Salivary gland adenoid cystic carcinoma: a review of chemotherapy and molecular therapies. Oral Oncol. *42*, 759–769. https://doi.org/10.1016/j.oraloncology.2006.01.001.

5. Warner, K.A., Adams, A., Bernardi, L., Nor, C., Finkel, K.A., Zhang, Z., McLean, S.A., Helman, J., Wolf, G.T., Divi, V., et al. (2013). Characterization of tumorigenic cell lines from the recurrence and lymph node metastasis of a human salivary mucoepidermoid carcinoma. Oral Oncol *49*, 1059–1066. https://doi.org/10.1016/j.oraloncology.2013.08.004.

6. Beltran, H., Eng, K., Mosquera, J.M., Sigaras, A., Romanel, A., Rennert, H., Kossai, M., Pauli, C., Faltas, B., Fontugne, J., et al. (2015). Whole-exome sequencing of metastatic cancer and biomarkers of treatment response. JAMA Oncol. *1*, 466–474. https://doi.org/10.1001/jamaoncol.2015.1313.

7. Rennert, H., Eng, K., Zhang, T., Tan, A., Xiang, J., Romanel, A., Kim, R., Tam, W., Liu, Y.C., Bhinder, B., et al. (2016). Development and validation of a whole-exome sequencing test for simultaneous detection of point mutations, indels and copy-number alterations for precision cancer care. NPJ Genom. Med. *1*, 16019. https://doi.org/10.1038/npjgenmed.2016.19.

8. Kato, S., Elkin, S.K., Schwaederle, M., Tomson, B.N., Helsten, T., Carter, J.L., and Kurzrock, R. (2015). Genomic landscape of salivary gland tumors. Oncotarget *6*, 25631–25645. https://doi.org/10.18632/oncotarget.4554.

9. Wang, K., Russell, J.S., McDermott, J.D., Elvin, J.A., Khaira, D., Johnson, A., Jennings, T.A., Ali, S.M., Murray, M., Marshall, C., et al. (2016). Profiling of 149 salivary duct carcinomas, carcinoma ex pleomorphic adenomas, and adenocarcinomas, not otherwise specified reveals actionable genomic alterations. Clin. Cancer Res. *22*, 6061–6068. https://doi.org/10.1158/1078-0432.Ccr-15-2568.

10. Wang, K., McDermott, J.D., Schrock, A.B., Elvin, J.A., Gay, L., Karam, S.D., Raben, D., Somerset, H., Ali, S.M., Ross, J.S., and Bowles, D.W. (2017). Comprehensive genomic profiling of salivary mucoepidermoid carcinomas reveals frequent BAP1, PIK3CA, and other actionable genomic alterations. Ann. Oncol. *28*, 748–753. https://doi.org/10.1093/annonc/mdw689.

11. Drost, J., and Clevers, H. (2017). Translational applications of adult stem cell-derived organoids. Development *144*, 968–975. https://doi.org/10.1242/dev.140566.

12. Pauli, C., Hopkins, B.D., Prandi, D., Shaw, R., Fedrizzi, T., Sboner, A., Sailer, V., Augello, M., Puca, L., Rosati, R., et al. (2017). Personalized in vitro and in vivo cancer models to guide precision medicine. Cancer Discov. *7*, 462–477. https://doi.org/10.1158/2159-8290.CD-16-1154.

13. Ishikawa, T., Ogawa, T., Nakanome, A., Yamauchi, Y., Usubuchi, H., Shiihara, M., Yoshida, T., Okamura, Y., Kinoshita, K., Katori, Y., and Furukawa, T. (2021). Whole exome sequencing and establishment of an organoid culture of the carcinoma showing thymus-like differentiation (CASTLE) of the parotid gland. Virchows Arch. *478*, 1149–1159. https://doi.org/10.1007/s00428-020-02981-8.

14. Shiihara, M., Ishikawa, T., Saiki, Y., Omori, Y., Hirose, K., Fukushige, S., Ikari, N., Higuchi, R., Yamamoto, M., Morikawa, T., et al. (2021). Development of a system combining comprehensive genotyping and organoid cultures for identifying and testing genotype-oriented personalised medicine for pancreatobiliary cancers. Eur. J. Cancer *148*, 239–250. https://doi.org/10.1016/j.ejca.2021.01.047.

15. Foschini, M.P., Marucci, G., and Eusebi, V. (2002). Low-grade mucoepidermoid carcinoma of salivary glands: characteristic immunohistochemical profile and evidence of striated duct differentiation. Virchows Arch. *440*, 536–542. https://doi.org/10.1007/s00428-001-0585-6.

16. Keysar, S.B., Eagles, J.R., Miller, B., Jackson, B.C., Chowdhury, F.N., Reisinger, J., Chimed, T.S., Le, P.N., Morton, J.J., Somerset, H.L., et al. (2018). Salivary gland cancer patient-derived xenografts enable characterization of cancer stem cells and new gene events associated with tumor progression. Clin. Cancer Res. *24*, 2935–2943. https://doi.org/10.1158/1078-0432.CCR-17-3871.

17. Alexandrov, L.B., Kim, J., Haradhvala, N.J., Huang, M.N., Tian Ng, A.W., Wu, Y., Boot, A., Covington, K.R., Gordenin, D.A., Bergstrom, E.N., et al. (2020). The repertoire of mutational signatures in human cancer. Nature *578*, 94–101. https://doi.org/10.1038/s41586-020-1943-3.

18. Takada, K., Aizawa, Y., Sano, D., Okuda, R., Sekine, K., Ueno, Y., Yamanaka, S., Aoyama, J., Sato, K., Kuwahara, T., et al. (2021). Establishment of PDX-derived salivary adenoid cystic carcinoma cell lines using organoid culture method. Int. J. Cancer *148*, 193–202. https://doi.org/10.1002/ijc.33315.

19. Alamri, A.M., Liu, X., Blancato, J.K., Haddad, B.R., Wang, W., Zhong, X., Choudhary, S., Krawczyk, E., Kallakury, B.V., Davidson, B.J., and Furth, P.A. (2018). Expanding primary cells from mucoepidermoid and other salivary gland neoplasms for genetic and chemosensitivity testing. Dis. Model. Mech. *11*, dmm031716. https://doi.org/10.1242/dmm.031716.

20. Driehuis, E., Kretzschmar, K., and Clevers, H. (2020). Establishment of patient-derived cancer organoids for drug-screening applications. Nat. Protoc. *15*, 3380–3409. https://doi.org/10.1038/s41596-020-0379-4.

21. Drost, J., and Clevers, H. (2018). Organoids in cancer research. Nat. Rev. Cancer *18*, 407–418. https://doi.org/10.1038/s41568-018-0007-6.

22. Seino, T., Kawasaki, S., Shimokawa, M., Tamagawa, H., Toshimitsu, K., Fujii, M., Ohta, Y., Matano, M., Nanki, K., Kawasaki, K., et al.

(2018). Human pancreatic tumor organoids reveal loss of stem cell niche factor dependence during disease progression. Cell Stem Cell *22*, 454–467.e6. https://doi.org/10.1016/j.stem.2017.12.009.

23. Ji, H., Ding, X., Zhang, W., Zheng, Y., Du, H., Zheng, Y., Song, H., Li, M., Jiang, Y., Xie, J., et al. (2020). Claudin-7 inhibits proliferation and metastasis in salivary adenoid cystic carcinoma through wnt/beta-catenin signaling. Cell Transplant. *29*. 963689720943583. https://doi.org/10.1177/0963689720943583.

24. Maimets, M., Rocchi, C., Bron, R., Pringle, S., Kuipers, J., Giepmans, B.N.G., Vries, R.G.J., Clevers, H., de Haan, G., van Os, R., and Coppes, R.P. (2016). Long-term in vitro expansion of salivary gland stem cells driven by Wnt signals. Stem Cell Rep. *6*, 150–162. https://doi.org/10.1016/j.stemcr.2015.11.009.

25. Tenório, J.D.R., da Silva, L.P., Xavier, M.G.D.A., Santana, T., do Nascimento, G.J.F., and Sobral, A.P.V. (2018). Differential expression of cyclooxygenase-2 and cyclin D1 in salivary gland tumors. Eur. Arch. Oto-Rhino-Laryngol. *275*, 2341–2347. https://doi.org/10.1007/s00405-018-5058-5.

26. Fujii, M., Shimokawa, M., Date, S., Takano, A., Matano, M., Nanki, K., Ohta, Y., Toshimitsu, K., Nakazato, Y., Kawasaki, K., et al. (2016). A colorectal tumor organoid library demonstrates progressive loss of niche factor requirements during tumorigenesis. Cell Stem Cell *18*, 827–838. https://doi.org/10.1016/j.stem.2016.04.003.

27. Sachs, N., de Ligt, J., Kopper, O., Gogola, E., Bounova, G., Weeber, F., Balgobind, A.V., Wind, K., Gracanin, A., Begthel, H., et al. (2018). A living biobank of breast cancer organoids captures disease heterogeneity. Cell *172*, 373–386.e10. https://doi.org/10.1016/j.cell.2017.11.010.

28. Bolhaqueiro, A.C.F., Ponsioen, B., Bakker, B., Klaasen, S.J., Kucukkose, E., van Jaarsveld, R.H., Vivié, J., Verlaan-Klink, I., Hami, N., Spierings, D.C.J., et al. (2019). Ongoing chromosomal instability and karyotype evolution in human colorectal cancer organoids. Nat. Genet. *51*, 824–834. https://doi.org/10.1038/s41588-019-0399-6.

29. Janku, F., Hong, D.S., Fu, S., Piha-Paul, S.A., Naing, A., Falchook, G.S., Tsimberidou, A.M., Stepanek, V.M., Moulder, S.L., Lee, J.J., et al. (2014). Assessing PIK3CA and PTEN in early-phase trials with PI3K/AKT/mTOR inhibitors. Cell Rep. *6*, 377–387. https://doi.org/10.1016/j.celrep.2013.12.035.

30. Hanna, G.J., Guenette, J.P., Chau, N.G., Sayehli, C.M., Wilhelm, C., Metcalf, R., Wong, D.J., Brose, M., Razaq, M., Pérez-Ruiz, E., et al. (2020). Tipifarnib in recurrent, metastatic HRAS-mutant salivary gland cancer. Cancer *126*, 3972–3981. https://doi.org/10.1002/cncr.33036.

31. Chen, C.H., Hsia, T.C., Yeh, M.H., Chen, T.W., Chen, Y.J., Chen, J.T., Wei, Y.L., Tu, C.Y., and Huang, W.C. (2017). MEK inhibitors induce Akt activation and drug resistance by suppressing negative feedback ERK-mediated HER2 phosphorylation at Thr701.

Mol. Oncol. *11*, 1273–1287. https://doi.org/10.1002/1878-0261.12102.

32. Balasis, M.E., Forinash, K.D., Chen, Y.A., Fulp, W.J., Coppola, D., Hamilton, A.D., Cheng, J.Q., and Sebti, S.M. (2011). Combination of farnesyltransferase and Akt inhibitors is synergistic in breast cancer cells and causes significant breast tumor regression in ErbB2 transgenic mice. Clin. Cancer Res. *17*, 2852–2862. https://doi.org/10.1158/1078-0432.CCR-10-2544.

33. Fushimi, C., Tada, Y., Takahashi, H., Nagao, T., Ojiri, H., Masubuchi, T., Matsuki, T., Miura, K., Kawakita, D., Hirai, H., et al. (2018). A prospective phase II study of combined androgen blockade in patients with androgen receptor-positive metastatic or locally advanced unresectable salivary gland carcinoma. Ann. Oncol. *29*, 979–984. https://doi.org/10.1093/annonc/mdx771.

34. Takahashi, H., Tada, Y., Saotome, T., Akazawa, K., Ojiri, H., Fushimi, C., Masubuchi, T., Matsuki, T., Tani, K., Osamura, R.Y., et al. (2019). Phase II trial of trastuzumab and docetaxel in patients with human epidermal growth factor receptor 2-positive salivary duct carcinoma. J. Clin. Oncol. *37*, 125–134. https://doi.org/10.1200/JCO.18.00545.

35. Sunami, K., Ichikawa, H., Kubo, T., Kato, M., Fujiwara, Y., Shimomura, A., Koyama, T., Kakishima, H., Kitami, M., Matsushita, H., et al. (2019). Feasibility and utility of a panel testing for 114 cancer-associated genes in a clinical setting: a hospital-based study. Cancer Sci. *110*, 1480–1490. https://doi.org/10.1111/cas.13969.

36. Yao, Y., Xu, X., Yang, L., Zhu, J., Wan, J., Shen, L., Xia, F., Fu, G., Deng, Y., Pan, M., et al. (2020). Patient-derived organoids predict chemoradiation responses of locally advanced rectal cancer. Cell Stem Cell *26*, 17–26.e6. https://doi.org/10.1016/j.stem.2019.10.010.

37. Brierly, J.D., Gospodarowicz, M.K., and Wittekind, C. (2017). UICC: TNM Classification of Malignant Tumours, 8th edition (Wiley Blackwell).

38. Broutier, L., Andersson-Rolf, A., Hindley, C.J., Boj, S.F., Clevers, H., Koo, B.K., and Huch, M. (2016). Culture and establishment of self-renewing human and mouse adult liver and pancreas 3D organoids and their genetic manipulation. Nat. Protoc. *11*, 1724–1743. https://doi.org/10.1038/nprot.2016.097.

39. McKenna, A., Hanna, M., Banks, E., Sivachenko, A., Cibulskis, K., Kernytsky, A., Garimella, K., Altshuler, D., Gabriel, S., Daly, M., and DePristo, M.A. (2010). The Genome Analysis Toolkit: a MapReduce framework for analyzing next-generation DNA sequencing data. Genome Res. *20*, 1297–1303. https://doi.org/10.1101/gr.107524.110.

40. Loh, J.W., Guccione, C., Di Clemente, F., Riedlinger, G., Ganesan, S., and Khiabanian, H. (2020). All-FIT: allele-frequency-based imputation of tumor purity from high-depth sequencing data. Bioinformatics *36*, 2173–2180. https://doi.org/10.1093/bioinformatics/btz865.

41. Tate, J.G., Bamford, S., Jubb, H.C., Sondka, Z., Beare, D.M., Bindal, N., Boutselakis, H., Cole, C.G., Creatore, C., Dawson, E., et al. (2019). COSMIC: the catalogue of somatic mutations in cancer. Nucleic Acids Res. *47*, D941–D947. https://doi.org/10.1093/nar/gky1015.

42. Landrum, M.J., Lee, J.M., Benson, M., Brown, G.R., Chao, C., Chitipiralla, S., Gu, B., Hart, J., Hoffman, D., Jang, W., et al. (2018). ClinVar: improving access to variant interpretations and supporting evidence. Nucleic Acids Res. *46*. D1062-d1067. https://doi.org/10.1093/nar/gkx1153.

43. Chakravarty, D., Gao, J., Phillips, S., Kundra, R., Zhang, H., Wang, J., Rudolph, J.E., Yaeger, R., Soumerai, T., Nissan, M.H., et al. (2017). OncoKB: a precision oncology knowledge base. JCO Precis. Oncol. *2017*, 1–16. https://doi.org/10.1200/PO.17.00011.

44. Tamborero, D., Rubio-Perez, C., Deu-Pons, J., Schroeder, M.P., Vivancos, A., Rovira, A., Tusquets, I., Albanell, J., Rodon, J., Tabernero, J., et al. (2018). Cancer Genome Interpreter annotates the biological and clinical relevance of tumor alterations. Genome Med. *10*, 25. https://doi.org/10.1186/s13073-018-0531-8.

45. Griffith, M., Spies, N.C., Krysiak, K., McMichael, J.F., Coffman, A.C., Danos, A.M., Ainscough, B.J., Ramirez, C.A., Rieke, D.T., Kujan, L., et al. (2017). CIViC is a community knowledgebase for expert crowdsourcing the clinical interpretation of variants in cancer. Nat. Genet. *49*, 170–174. https://doi.org/10.1038/ng.3774.

46. Sondka, Z., Bamford, S., Cole, C.G., Ward, S.A., Dunham, I., and Forbes, S.A. (2018). The COSMIC Cancer Gene Census: describing genetic dysfunction across all human cancers. Nat. Rev. Cancer *18*, 696–705. https://doi.org/10.1038/s41568-018-0060-1.

47. Sanchez-Vega, F., Mina, M., Armenia, J., Chatila, W.K., Luna, A., La, K.C., Dimitriadoy, S., Liu, D.L., Kantheti, H.S., Saghafinia, S., et al. (2018). Oncogenic signaling pathways in the cancer genome Atlas. Cell *173*, 321–337.e10. https://doi.org/10.1016/j.cell.2018.03.035.

48. Riester, M., Singh, A.P., Brannon, A.R., Yu, K., Campbell, C.D., Chiang, D.Y., and Morrissey, M.P. (2016). PureCN: copy number calling and SNV classification using targeted short read sequencing. Source Code Biol. Med. *11*, 13. https://doi.org/10.1186/s13029-016-0060-z.

49. Talevich, E., Shain, A.H., Botton, T., and Bastian, B.C. (2016). CNVkit: genome-wide copy number detection and visualization from targeted DNA sequencing. PLoS Comput. Biol. *12*, e1004873. https://doi.org/10.1371/journal.pcbi.1004873.

50. Venkatraman, E.S., and Olshen, A.B. (2007). A faster circular binary segmentation algorithm for the analysis of array CGH data. Bioinformatics *23*, 657–663. https://doi.org/10.1093/bioinformatics/btl646.

51. Olshen, A.B., Bengtsson, H., Neuvial, P., Spellman, P.T., Olshen, R.A., and Seshan, V.E. (2011). Parent-specific copy number in paired tumor-normal studies using circular binary segmentation. Bioinformatics *27*, 2038–2046. https://doi.org/10.1093/bioinformatics/btr329.

52. Ge, S.X., Son, E.W., and Yao, R. (2018). iDEP: an integrated web application for differential expression and pathway analysis of RNA-Seq data. BMC Bioinf. *19*, 534. https://doi.org/10.1186/s12859-018-2486-6.

53. Uhrig, S., Ellermann, J., Walther, T., Burkhardt, P., Fröhlich, M., Hutter, B., Toprak, U.H., Neumann, O., Stenzinger, A., Scholl, C., et al. (2021). Accurate and efficient detection of gene fusions from RNA sequencing data. Genome Res. *31*, 448–460. https://doi.org/10.1101/gr.257246.119.

54. Noda, H., Okumura, Y., Nakayama, T., Miyabe, S., Fujiyoshi, Y., Hattori, H., Shimozato, K., and Inagaki, H. (2013). Clinicopathological significance of MAML2 gene split in mucoepidermoid carcinoma. Cancer Sci. *104*, 85–92. https://doi.org/10.1111/cas.12039.

55. Skalova, A., Vanecek, T., Martinek, P., Weinreb, I., Stevens, T.M., Simpson, R.H.W., Hyrcza, M., Rupp, N.J., Baneckova, M., Michal, M., Jr., et al. (2018). Molecular profiling of mammary analog secretory carcinoma revealed a subset of tumors harboring a novel ETV6-RET translocation: report of 10 cases. Am. J. Surg. Pathol. *42*, 234–246. https://doi.org/10.1097/pas.0000000000000972.

56. Hammond, M.E.H., Hayes, D.F., Dowsett, M., Allred, D.C., Hagerty, K.L., Badve, S., Fitzgibbons, P.L., Francis, G., Goldstein, N.S., Hayes, M., et al. (2010). American society of clinical oncology/college of American pathologists guideline recommendations for immunohistochemical testing of estrogen and progesterone receptors in breast cancer. J. Clin. Oncol. *28*, 2784–2795. https://doi.org/10.1200/JCO.2009.25.6529.

57. Ritz, C., Baty, F., Streibig, J.C., and Gerhard, D. (2015). Dose-response analysis using R. PLoS One *10*, e0146021. https://doi.org/10.1371/journal.pone.0146021.

iScience
Article

CellPress
OPEN ACCESS

STAR★METHODS

KEY RESOURCES TABLE

REAGENT or RESOURCE	SOURCE	IDENTIFIER
Antibodies		
Rabbit monoclonal anti-Androgen Receptor (clone SP107)	Roche	Cat#760-4605 RRID: AB_2921271
Mouse monoclonal anti-αSMA (clone 1A4)	Agilent Technologies	Cat# M0851, RRID: AB_2223500
Mouse monoclonal anti-CD44 (F-4)	Santa Cruz Biotechnology Inc.	Cat#sc-9960, RRID: AB_627066
Rabbit polyclonal anti-c-kit	Agilent Technologies	Cat#A4502, RRID: AB_2335702
Mouse monoclonal anti-CK 7 (clone LP5K)	Agilent Technologies	Cat# sc-53264, RRID:AB_784188
Rabbit monoclonal anti-CK14 (clone SP53)	Roche	Cat#760-4805, RRID: AB_2935819
Mouse monoclonal anti-GCDFP15 (clone D6)	SIGNET	Cat# SIG-3611-1000, RRID:AB_662894
Rabbit polyclonal anti-HER2	Agilent Technologies	Cat# SK00121-5, RRID: AB_2935822
Mouse monoclonal anti-Ki-67 (clone MIB-1)	Agilent Technologies	Ca#M7240, RRID:AB_2142367
Mouse monoclonal anti-laminin (clone LAM-89)	Leica	Cat# NCL-LAMININ, RRID:AB_563849
anti-p40 (clone BC28)	Roche	Cat#790-4950, RRID:AB_2935820
Mouse monoclonal anti-p53 (clone DO7)	Roche	Cat# 05278775001, RRID:AB_2892528
anti-p63 (clone 4A4)	Roche	Cat#790-4509, RRID: AB_2335989
Mouse monoclonal anti-pan-CK (clone AE1/AE3 and PCK26)	Roche	Cat# 760-2135, RRID:AB_2810237
Mouse monoclonal anti-type IV collagen (clone CIV22)	Agilent Technologies	Cat# M0785, RRID:AB_2082944
Rabbit polyclonal anti-Phospho-p44/42 MAPK (Erk1/2) (Thr202/Tyr204)	Cell Signaling Technology	Cat# 9101, RRID:AB_331646
Rabbit monoclonal anti-ERK (clone 137F5)	Cell Signaling Technology	Cat# 4695, RRID:AB_390779
Rabbit monoclonal anti-AKT (clone C67E7)	Cell Signaling Technology	Cat# 4691, RRID:AB_915783
anti-phospho-AKT(Ser473) (clone D9E)	Cell Signaling Technology	Cat# 4060, RRID:AB_2315049
anti-β-actin (clone AC-15)	Sigma-Aldrich	Cat# A1978, RRID:AB_476692
Biological samples		
293T-HA-Rspo1-Fc	TREVIGEN	Cat# 3710-001-01
L Wnt-3A	ATCC	ATCC 2647
Chemicals, peptides, and recombinant proteins		
Advanced DMEM/F-12	Thermo Fisher Scientific	Cat# 12634-010
DMEM, high glucose, GlutaMAX, pyruvate	Thermo Fisher Scientific	Cat# 31966-021
GlutaMAX	Thermo Fisher Scientific	Cat# 35050-068
HEPES	Thermo Fisher Scientific	Cat# 15630-056
Penicillin/streptomycin 10,000 U/ml	Thermo Fisher Scientific	Cat# 15140-122
Collagenase from *Clostridium histolyticum*	Sigma-Aldrich	Cat# C9407
DispaseII	Thermo Fisher Scientific	Cat# 17105-041
DNaseI	Sigma-Aldrich	Cat# DN25
Cultrex Reduced Growth Factor Basement Membrane Extract (BME), Type 2, PathClear	R&D Systems	Cat# 3533-010-02
B27 Supplement	Thermo Fisher Scientific	Cat# 12587-010
N2 supplement	Thermo Fisher Scientific	Cat# 17502-048

(Continued on next page)

Continued

REAGENT or RESOURCE	SOURCE	IDENTIFIER
N-acetyl-L-cysteine	Sigma-Aldrich	Cat# A9165
Nicotinamide	Sigma-Aldrich	Cat# N0636
[Leu15]-Gastrin I human	Sigma-Aldrich	Cat# G9145
Recombinant human EGF	Peprotech	Cat# AF-100-15
Recombinant human FGF-10	Peprotech	Cat#100-26
A83-01	Cellagen Tech	Cat# C2831-2
PGE-2	Cayman Chemical	Cat# 14010
Y-27632	Nacalai Tesque	Cat# 18188-04
Dexamethasone	Sigma-Aldrich	Cat# D4902
Recombinant human Noggin	Peprotech	Cat# 120-03
TrypLE Express	Thermo Fisher Scientific	Cat# 12605-028
Recovery Cell Culture Freezing Medium	Thermo Fisher Scientific	Cat# 12648-010
iPGell	GenoStaff	Cat# PG20-1
Platinum PCR SuperMix High Fidelity	Thermo Fisher Scientific	Cat# 12532016
ExoSAP-IT	Thermo Fisher Scientific	Cat# 78250
Big Dye Terminator Cycle Sequencing Kit	Thermo Fisher Scientific	Cat# 433745
Agencourt CleanSEQ	Beckman Coulter	Cat# A29151
AccuPrime Taq DNA Polymerase System	Invitrogen	Cat# 12339016
ZytoLight SPEC MAML2 Dual Color Break Apart Probe	ZytoVision	Cat# Z-2014-200
PathVysion HER-2 DNA Probe Kit	Abbott	Cat# 02J01-030
alamarBlue Cell Viability Reagent	Thermo Fisher Scientific	Cat# DAL1025
Cisplatin	Fujifilm Wako	Cat# 033-20091
Rapamycin	Selleck	Cat# S1039
Selumetinib	Selleck	Cat# S1008
Tipifarnib	Selleck	Cat# S1453
Bicalutamide	Santa Cruz Biotechnology	Cat# sc-202976
Trastuzumab	Pfizer	Cat# 2117990
Critical commercial assays		
DNeasy Blood and Tissue Kit	QIAGEN	Cat# 69506
RNeasy Mini Kit	QIAGEN	Cat# 74104
Transcriptor First Strand cDNA Synthesis Kit	Roche	Cat# 04897030001
Deposited data		
Transcriptome sequence: Raw and analyzed data	This paper	GEO: GSE223554
Unprocessed data	This paper	Mendeley Data: https://data.mendeley.com/datasets/s2njncjd5s/draft?a=dee7fe11-ec58-4475-b1b2-745a8c77407f
Oligonucleotides		
Primers for Sanger sequence and RT-PCR, see Table S15	This paper	N/A
Software and algorithms		
R for Mac (3.5.2 GUI 1.70 El Capitan build (7612)	S. Urbanek & H.-J. Bibiko	http://www.R-project.org
ImageJ2 2.9.0	Wayne Rasband	https://imagej.nih.gov/ij/

RESOURCE AVAILABILITY

Lead contact

Further information and requests for resources and reagents should be directed to and will be fulfilled by the lead contact, Toru Furukawa (toru.furukawa@med.tohoku.ac.jp).

Materials availability

There are restrictions to the availability of cultured cells due to limited quantity.

Data and code availability

- Transcriptome data have been deposited at GEO (GSE223554) and are publicly available as of the date of publication. Original western blotting images, the data for the mutational signature chart, unprocessed data for cell viability assay and ImageJ analysis have been deposited at Mendeley Data and are publicly available as of the date of publication. Accession number is listed in the key resources table.

- This paper does not report original code.

- Any additional information required to reanalyze the data reported in this paper is available from the lead contact upon request.

EXPERIMENTAL MODEL AND SUBJECT DETAILS

In this study, we enrolled patients with salivary gland tumors or non-squamous cell carcinomas in the head and neck regions. The clinicopathological features of patients were shown in Table S1 including sex. This study was approved by the ethical committee of the Tohoku University Graduate School of Medicine (#2019-1-082), and all patients involved in this study provided written informed consent. All procedures involving human participants in this study were in accordance with the ethical standards of the institutional research committee and with the 1964 Helsinki Declaration. The influence of sex in this study was unknown.

METHOD DETAILS

Processing patients' materials

Tumors with normal salivary gland tissues were surgically resected at Tohoku University Hospital. The tissues were pathologically evaluated based on the TNM classification of the Union of International Cancer Control and the WHO classification.[37] The specimens were divided into three parts to be processed for pathology, nucleic acid extraction, and primary culture. In addition, part of the tumor biopsy specimen was collected to establish the primary culture. Biopsy was performed using a sterile 18-gauge aspiration kit (TSK Laboratories, Tokyo, Japan) under ultrasonographic guidance.

Organoid and monolayer cultures

Organoid-cultured cells (organoids) and monolayer-cultured cells (2D cells) were established from fresh surgical specimens of primary tumors according to protocols described previously with modifications as follows.[13,14,38] A portion of the fresh surgical specimen was collected in the ice-cold basal medium (advanced Dulbecco's modified Eagle's medium (DMEM)/F-12 supplemented with 1% penicillin/streptomycin, 1% GlutaMAX, and 10 mM HEPES [Thermo Fisher Scientific, Carlsbad, CA, USA]).[38] The specimen was minutely cut, washed several times with the wash medium (DMEM, high glucose, with 1% GlutaMAX and 1mM pyruvate [Thermo Fisher Scientific] supplemented with 1% fetal bovine serum [Sigma-Aldrich, St. Louis, MO, USA] and 1% penicillin/streptomycin),[38] incubated in the digestion solution (the wash medium with 0.125 mg/mL collagenase [Sigma-Aldrich], 0.125 mg/mL dispase II [Thermo Fisher Scientific], and 0.1 mg/mL DNase I [Sigma-Aldrich])[38] for 1-6 h at 37°C, and monitored every 30 min to prevent over-digestion. The digested tissue was pelleted by centrifugation at 300 × g for 5min at room temperature (RT). The pellet was washed twice with the wash medium and basal medium sequentially, and pelleted by centrifugation at 300 × g for 5min at RT. The number of cells was not counted on the time of initial spread because tumor specimens were not completely digested into single cells. The resulting pellets were divided into two tubes for organoid and monolayer culture.

In the organoid culture, the resulting pellet was resuspended in ice-cold Cultrex Reduced Growth Factor Basement Membrane Extract (BME), Type 2, PathClear (R&D Systems, Minneapolis, MN, USA), and then 50 μL were dropped into the center of a well of a 24-well plate. After the BME solidified, the droplet was

overlaid with 500 μL of culture medium (the basal medium supplemented with 1:50 B27 supplement [Thermo Fisher Scientific], 1:100 N2 supplement [Thermo Fisher Scientific], 1 mM N-acetyl-L-cysteine [Sigma-Aldrich], 10 mM nicotinamide [Sigma-Aldrich], 10 nM recombinant human [Leu15]-gastrin I [Sigma-Aldrich], 50 ng/mL recombinant human EGF [PeproTech, Cranbury, NJ, USA], 100 ng/mL recombinant human FGF10 [PeproTech], 5 μM A83-01 [Cellagen Technology, San Diego, CA, USA], 3 μM PGE-2 [Cayman Chemical, Ann Abor, MI, USA], 10 mM Y-27632 [Nacalai Tesque, Kyoto, Japan], and 3 nM dexamethasone [Sigma-Aldrich]). Culture medium with 30% (vol/vol) Wnt3a-conditioned medium, 5% (vol/vol) Rspo1-conditioned medium, and 25 ng/mL recombinant human Noggin (PeproTech) were also used as the full medium. The culture medium was changed twice a week. The passage was performed every 7-21 days after plating. For passage, organoids were collected from the plate by disrupting the BME droplets with a 1,000 μL pipette tip and washed in 5-10 mL phosphate buffered saline (PBS). The pellet was resuspended in 1 mL of TrypLE Express (Thermo Fisher Scientific) supplemented with 10 μM Y27632 and incubated at 37°C for 5-15 min. The cells were subsequently resuspended in ice-cold BME and plated in appropriate splits (1:3 - 1:6) to allow efficient outgrowth of new organoids.

In the monolayer culture, the pellet was resuspended in the culture medium and 2 mL of the cell suspension was plated per well of a 6-well plate for conventional monolayer culture without any coating. 2D cells were passaged when they reached 70%-90% confluency. For passage, the culture medium was removed, and the cells were rinsed with PBS and then incubated with 0.05% trypsin. After trypsinization and centrifugation, the resulting pellet was resuspended in culture medium and plated by splitting in appropriate splits (1:2 - 1:6) to allow efficient growth. The growing cells that adhered to the dish were passaged as 2D cells, and when viable floating tissues and cells formed spheroids, they were collected and spread as the organoids culture at the first passage (Figure S1). Freezing stock was prepared using recovery cell culture freezing medium (Thermo Fisher Scientific).

For histological examination, organoids were collected from the plate and solidified without changing their structure using iPGell (GenoStaff, Tokyo, Japan) as previously described.[13] Organoids and 2D cells were used at passages 2-5 for the histological and genetic examination.

WES and sanger sequencing

DNA was extracted using the DNeasy Blood and Tissue Kit (QIAGEN, Hilden, Germany) from fresh-frozen tissues with appropriate microdissection and cultured cells according to the manufacturer's instructions. Non-tumoral tissues from corresponding patients (typically, the submandibular or parotid gland) were used as a reference to detect somatic alterations in the tumor. WES was performed by Macrogen Japan Corp. (Kyoto, Japan) or Tohoku University Tohoku Medical Megabank Organization using SureSelect Human All Exon V6 (Agilent Technologies, Santa Clara, CA, USA) and NovaSeq 6000 or HiSeq 2500 (Illumina Inc., San Diego, CA, USA) using the paired-end sequencing method. Sequencing data were mapped with BWA-MEM 0.1.17. Somatic and germline variation calls were performed by GATK 4.1.1, and annotations were added by using SnpEff 4.3t with GENCODE29. Somatic copy number alterations (CNAs) were identified through somatic copy number variant discovery using GATK.[39] Variants with fewer than four calls were considered unreliable and were therefore dismissed. Tumor cell purity was estimated using an allele-frequency-based imputation method.[40] Candidate driver mutations were defined as mutations with over 10 calls in COSMIC,[41] pathogenic or likely pathogenic in ClinVar,[42] oncogenic or likely oncogenic in OncoKB,[43] Cancer Genome Interpreter,[44] or CIViC;[45] or loss-of-function mutations of the tumor suppressor genes listed in the COSMIC Census Gene.[46] The detected somatic alterations were classified as canonical oncogenic signaling pathways.[47] Sanger sequencing was performed as follows. DNA was amplified with Platinum™ PCR Super-Mix High Fidelity (Thermo Fisher Scientific) and primers listed in Table S15. The amplified products were treated with ExoSAP-IT (Thermo Fisher Scientific). The treated products were subjected to a dideoxy chain-terminating reaction using Big Dye Terminator Cycle Sequencing Kit (Thermo Fisher Scientific), purification with Agencourt CleanSEQ (Beckman Coulter, Brea, CA), and then capillary-electrophoresed using a 3500xL Genetic Analyzer (Thermo Fisher Scientific). All procedures were performed in accordance with the manufacturers' protocol. PureCN and cnvkit were used to describe copy number alterations on global chromosome.[48–51]

Whole transcriptome sequencing analysis

Total RNA was isolated using the RNeasy Mini Kit (QIAGEN) according to the manufacturer's instructions. The isolated RNA was constructed into a fragment library using the TruSeq Stranded Total RNA LT Sample

Prep Kit Gold (Illumina). The constructed libraries were subjected to total transcriptome enrichment using a NovaSeq 6000 S4 Reagent Kit. The prepared transcriptome libraries were sequenced on an Illumina NovaSeq 6000 platform using the paired-end sequencing method. All procedures were performed according to the manufacturer's instructions. The reads were aligned to the USCS hg19 human RefSeq transcriptome using the HISAT2. Approximately 100 million reads were mapped for each sample. Known genes and transcripts were assembled using StringTie based on a reference genome model. iDEP (http://bioinformatics.sdstate.edu/idep/) was used for hierarchical clustering, enrichment analysis, and principal component analysis.[52] Fusion gene analysis was performed using Arriba.[53] Transcriptome data is available from the Gene Expression Omnibus under accession number of GSE223554.

RT-PCR to detect fusion genes

RNA was extracted from fresh-frozen tissues and cultured cells using an RNeasy Mini Kit (QIAGEN). Complementary DNA (cDNA) was synthesized using 50-500 ng of RNA and the Transcriptor First Strand cDNA Synthesis Kit (Roche, Basel, Switzerland). RT-PCR was performed to detect fusion transcripts of *CRTC1-MAML2*, *CRTC3-MAML2*, *ETV6-NTRK3*, and *ETV6-RET* using 2 µL cDNA in a reaction consisting of 0.5 µL AccuPrime Taq, 2.5 µL 10×AccuPrime PCR Buffer I (Invitrogen, Carlsbad, CA, USA), and 10 pmol of each pair of primers listed in Table S15.[54,55]

Histopathology, immunohistochemistry, and fluorescent *in situ* hybridization (FISH)

Hematoxylin and eosin (HE) staining, Alcian blue and periodic acid-Schiff (AB-PAS) staining, and immunohistochemical stainings were performed on 4-µm-thick sections of formalin-fixed paraffin-embedded primary tissues and organoids. Immunohistochemistry (IHC) was performed using the following primary antibodies: anti-AR (SP107, ready-to-use, Roche), anti-αSMA (1A4, 1:800, Agilent Technologies), anti-CD44 (F-4, 1:100, Santa Cruz Biotechnology, Santa Cruz, CA, USA), anti-c-kit (polyclonal, 1:200, Agilent Technologies), anti-cytokeratin (CK) 7 (LP5K, 1:500, Santa Cruz Biotechnology), anti-CK14 (SP53, ready-to-use, Roche), anti-GCDFP15 (D6, 1:200, SIGNET, San Francisco, CA, USA), anti-HER2 (polyclonal (Herceptest), ready-to-use, Agilent Technologies), anti-Ki-67 (MIB-1, ready-to-use, Agilent Technologies), anti-laminin (LAM-89, 1:3000, Leica, Wetzlar, Germany), anti-p40 (BC28, ready-to-use, Roche), anti-p53 (DO7, ready-to-use, Roche), anti-p63 (4A4, ready-to-use, Roche), anti-pan-CK (AE1/AE3 and PCK26, ready-to-use, Roche), anti-S-100 (15E2E2, 1:10, Biogenex, Fremont, CA, USA), and anti-type IV collagen (CIV22, 1:100, Agilent Technologies). A Histofine SAB-PO kit (Nichirei Bioscience, Tokyo, Japan) was used to detect anti-αSMA, anti-CD44, anti-c-kit, anti-CK7, anti-GCDFP15, anti-laminin, anti-S-100, and anti-type IV collagen. The Benchmark Ultra system (Ventana Medical Systems, Tuscon, AZ, USA) was used to detect anti-AR, anti-CK14, anti-p40, anti-p53, anti-p63, and anti-pan-CK. Autostainer Link48 (Agilent Technologies) was used for anti-HER2 and anti-Ki-67 antibodies. The HER2 expression scores were determined as previously described.[56] *MAML2*-FISH and *HER2/ERBB2*-FISH were performed on unstained 4-µm-thick FFPE sections using the ZytoLight SPEC MAML2 Dual Color Break Apart Probe (ZytoVision, Bremerhaven, Germany) and the PathVysion HER-2 DNA Probe Kit (Abbott, Chicago, IL, USA), respectively, according to the manufacturer's protocol. Appropriate positive and negative controls were also included.

Immunoblotting

Total cell lysates were prepared by using RIPA buffer (Sigma-Aldrich) supplemented with CompleteMini and PhosStop (Roche). Protein concentrations were measure by using DC-protein assay kit (Bio Rad, Hercules, CA, USA.). The total cell lysates were analyzed using electrophoresis on a 10–20% gradient polyacrylamide gel and transferred onto a polyvinylidene difluoride membrane (ATTO; Tokyo, Japan) using the XV Pantera MP System (DRC Co. Ltd.; Tokyo, Japan), according to the manufacturers' protocol. The primary antibodies used were polyclonal anti-Phospho-p44/42 MAPK (Erk1/2) (Thr202/Tyr204) (1:1500; Cell Signaling Technology, Danvers, MA, USA), monoclonal anti-ERK (p44/42 MAPK; Erk1/2) (137F5; 1:1500; Cell Signaling Technology), anti-AKT (C67E7, 1:1500, Cell Signaling Technology), anti-phospho-AKT (Ser473) (D9E, 1:1500, Cell Signaling Technology), and anti-β-actin (AC-15, 1:1000, Sigma-Aldrich).

Cell viability assay with patient-derived cancer organoids and monolayer culture cells

Organoid cells were counted, and 10,000 single cells were embedded in 30 µL of BME and plated per well in a 48-well plate containing 250 µL of growth medium. Two days after plating, the viability of organoids was quantified using the AlamarBlue Cell Viability Reagent (Thermo Fisher Scientific) and a microplate reader (Spectra Max M2e, Molecular Devices, San Jose, CA, USA), according to the manufacturers' protocols.

After the first assay, the medium was replaced with growth medium supplemented with drugs for targeted therapy experiments. The drugs used were cisplatin (Fujifilm Wako, Osaka, Japan), rapamycin (Selleck Chemicals LLC, Houston, TX, USA), selumetinib (AZD6244) (Selleck Chemicals LLC), tipifarnib (Selleck Chemicals LLC), bicalutamide (Santa Cruz Biotechnology Inc.), and trastuzumab (Pfizer, New York, NY, USA). The concentration of dimethyl sulfoxide in the medium supplemented with drugs did not exceed 0.1%, and was adjusted to 0.1% in the control. To investigate the effects of the drugs, the viability of organoids was quantified after six days of treatment with cisplatin and every two days for six days of treatment with molecular-targeted drugs. In the assay with 2D cells, cells were counted and 10,000 cells were spread on a 96-well plate with 200 μL of the same growth medium used for organoids, and the cell viability assay was performed in the same way as for organoids. All experiments were performed at least twice, and each assay included at least three independent wells for each condition. Dose-response curves with IC50 values were described by an R package, drc,[57] using the relative proliferation on day six compared to the first assay.

Imaging analysis

To validate the Alamar Blue assay results, we used the software, ImageJ for mac (version 2.0.0-rc-69/1.52p) to analyze the number of clusters and the cell density in culture images taken in the Alamar Blue assay. Alamar blue assay and the imaging analysis showed positive correlations in both organoids and 2D cells (Organoids, $p < 2.2e-16$, rho = 0.83; 2D cells, $p = 0.0002$, rho = 0.72, Figure S8).

QUANTIFICATION AND STATISTICAL ANALYSIS

Student's t-test was used to determine the significance of differences in quantitative variables. Fisher's exact test was used to determine the significance of differences in categorical data. Spearman's rank correlation test was used to determine the significance of two nonparametric two variables. Asterisks represents two-sided p values less than 0.05. All statistical analyses were computed using R for Mac (3.5.2 GUI 1.70 El Capitan build (7612)).